FABRICATION OF A SURFACE PLASMON RESONANCE PLATFORM

FOR THE DEVELOPMENT OF AN ELECTROKINTIC SURFACE PLASMON

RESONANCE (EK-SPR) BIOSENSOR

by

Ornella Sathoud

A dissertation submitted to the Faculty of the University of Delaware in partial fulfillment of the requirements for the degree of Doctor of Philosophy in Chemistry and Biochemistry

Fall 2018

FABRICATION OF A SURFACE PLASMON RESONANCE PLATFORM FOR THE DEVELOPMENTOF AN ELECTROKINTIC SURFACE PLASMON RESONANCE (EK-SPR) BIOSENSOR

by

Ornella Sathoud

Approved: _____
Brian J. Bahnson, Ph.D.
Chair of the Department of Chemistry and Biochemistry

Approved: _____
John A. Pelesko, Ph.D.
Interim Dean of the College of Arts and Sciences

Approved: _____
Douglas J. Doren, Ph.D.
Interim Vice Provost for the Office of Graduate and Professional Education

I certify that I have read this dissertation and that in my opinion it meets the academic and professional standard required by the University as a dissertation for the degree of Doctor of Philosophy.

Signed: _____

Karl S. Booksh, Ph.D.
Professor in charge of dissertation

I certify that I have read this dissertation and that in my opinion it meets the academic and professional standard required by the University as a dissertation for the degree of Doctor of Philosophy.

Signed: _____

Steven D. Brown, Ph.D.
Member of dissertation committee

I certify that I have read this dissertation and that in my opinion it meets the academic and professional standard required by the University as a dissertation for the degree of Doctor of Philosophy.

Signed: _____

Tatyana Polenova, Ph.D.
Member of dissertation committee

I certify that I have read this dissertation and that in my opinion it meets the academic and professional standard required by the University as a dissertation for the degree of Doctor of Philosophy.

Signed: _____

Jacqueline Fajardo, Ph.D.
Member of dissertation committee

I certify that I have read this dissertation and that in my opinion it meets the academic and professional standard required by the University as a dissertation for the degree of Doctor of Philosophy.

Signed: _____

Nii O. Attoh-Okine, Ph.D.
Member of dissertation committee

ACKNOWLEDGMENTS

Many thanks to those who supported and inspired my doctoral journey. First, I wish to acknowledge my adviser, Karl Booksh, his guidance and my growth and as a researcher and individual. Through our journey together I have developed a better sense of independence and resourcefulness that strengthen my self-confidence in my decisions making process through research and life. I also thank my colleagues in the Booksh lab, for their discussion and intellectual contribution to my progress. Thank you to the Department of Chemistry and Biochemistry at University of Delaware, faculty and staff for providing an environment for personal and intellectual growth. Thank you to Susan Cheadle for her countless administrative help. I would like to thank my committee members for sharing their wisdom regarding the doctoral process. Thank you to my family, friends, many mentors and health professionals who contributed to the completion of this journey; their help, love and understanding provided me with the necessary mental, spiritual and emotional balance, to make it this far. I will never thank my parents enough for going above and beyond, *far from the eyes but never from the heart*. Thank you to my siblings Julie-Anne, Jean-Felix and Olivier, my mentees Rose Adrianna and Franklin, my MVJ team Coach Greg, Jason Schmelle, Adonis and Zy, my mentors Dr Neal, Dr Okine, and Dr Kalumbu, and my counselors Dr Tsukada and Dr Murphy for always reminding me of my strengths and value in my darkest moments and never letting me quit. A special thanks to Dr Sharon Neal and Dr Jolie Blake for being inspiring role models, always willing to share their knowledge and reminding me that it

can be done. Thank you for teaching me how to find peace in my work and reconnecting with my love for science.

TABLE OF CONTENTS

LIST OF TABLES

LIST OF FIGURES

ABSTRACT

Point-of-Care Testing (POCT) is a clinical analysis performed near the patient, rather than in a remote, dedicated laboratory. POCT is typically performed by non-laboratory personnel and the results are used for clinical decision-making. Acute Coronary syndrome (ACS) is a group of conditions that considerably decreases or stops blood flow to the heart muscle, causing the heart to be damaged or stressed. Such events cause the release of biomarkers into the blood stream. Myocardial Infarction (MI), commonly called “heart attack”, is a well-known ACS that is diagnosed by measuring the change in the level of cardiac biomarkers (preferably troponin) in the blood. This dissertation presents the fabrication of a platform to be adapted as a point-of care sensor with surface plasmon resonance as the detection method. 4-aminophenylalanine is electrografted on the gold sensing surface as the linker to allow receptors immobilization on the sensing surface. Electrokinetic method is to be combined with surface plasmon resonance, to enhance the sensitivity and selectivity of a cardiac protein biosensor. Surface Plasmon Resonance (SPR) is a real time, label free optical method that measures the refractive index change when the analyte binds receptors immobilized at the surface of a metal, here gold. In this report details on how electrografting of 4-aminophenylalanine on gold thin film permits the fabrication of an SPR biosensor platform that could possibly be as a troponin biosensor. An overview on the sensing surface characterization to confirm surface modification is offered as well as the sensor performance using bovine serum albumin bovine serum albumin antibodies.

Chapter 1

INTRODUCTION

1.1 Dissertation Overview

Cardiovascular disease (CVD) and stroke causes enormous health and economic burdens in the United States and globally. Coronary heart disease (CHD) is the leading cause of deaths attributable to CVD in the United States. 43.8% of CVD deaths can be attributed to CHD, followed by stroke with 16.8%, high blood pressure with 9.4%), heart failure with 9.0%, diseases of the arteries with 3.1%, and other CVDs (17.9%) [1]. Every 40 seconds in the U.S. someone will have a stroke or heart attack, based on the American Heart Association (AHA) computation. Heart attacks or AMI is the world's leading cause of mortality and morbidity, with an average of 8.9 million deaths reported in the United States only in 2015 by the American Heart Association[1]. Acute coronary syndrome (ACS) is a subcategory of CHD, which occurs when blood flow to the heart is reduced, thereby reducing myocardial cells oxygen supply; it can be caused by the rupture of unstable atherosclerotic plaques which induces thrombus formation and leads to the occlusion of a coronary artery. The two primary types of ACS include unstable angina (UA) in which the myocardial cells are reversibly damaged and acute myocardial infarction (AMI) in which myocardial cells are irreversibly damaged (myocardial cell death) due to blood flow being completely blocked[2,3]. AMI has a high misdiagnosis or delayed diagnosis rate, causing inappropriate hospital discharge or unnecessary

hospitalization, resulting in billions of dollars in hospitals bills. This issue rings the alarm on the importance of developing quick and reliable diagnostics for AMI[4,5].

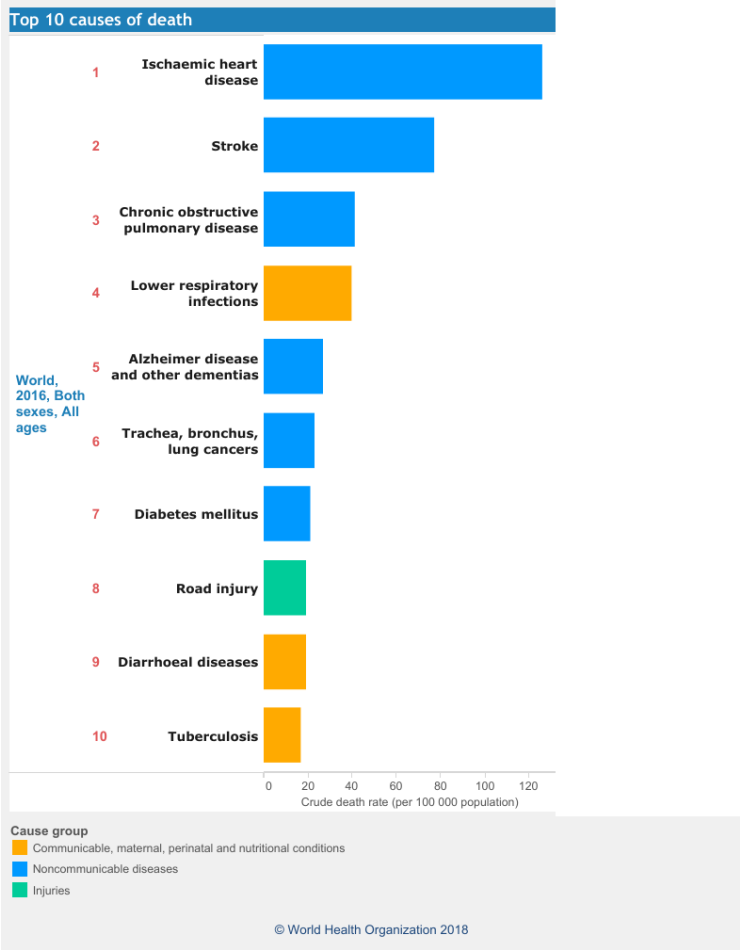

Figure 1.1 World top 10 causes of death in 2016 by the World Health Organization (WHO)[6] (Figure 1.1 not mentioned in the text)

The diagnosis of AMI starts with the patient physical examination followed by the quantification of the biological markers released upon cardiac tissue, muscle or cell

death. The extent of the damage and the location of the dead tissue, muscle or cell can be determined by the amount and type of biomarkers released in the blood stream or other possible biological fluid. Some biomarkers of interest for an AMI diagnosis have been: myoglobin, cardiac troponin I, creatine kinase myocardial band (CK-MB), C-reactive protein, lactate dehydrogenase (LDH) and more. During a cardiac event the concentration of previously listed molecule rise above the identified healthy average. Different biomarkers have different lifetime in the bloodstream that help with an accurate diagnostic. The protein troponin, also known as the troponin complex, consist of three regulatory proteins: troponin C (TnC), troponin T (TnT), and troponin I (TnI). Troponin is part of the heart muscle contractile apparatus. The presence of troponin in the circulation at levels above a good indication of damage to cardiac cells, such as but not limited to AMI. Troponins are very sensitive and specific indicators of cardiac injury. Just like other cardiac markers, observation of a rise and fall in troponin levels in a suitable time-frame increases the diagnostic accuracy of acute myocardial infarction. Troponins start to rise approximately 4-6 h after the onset of acute myocardial infarction and peak at approximately 24 h, as is the case with creatine kinase-MB. They remain elevated for 7-10 days giving a longer diagnostic window than creatine kinase. Cardiac troponin I (cTnI) and troponin T(cTnT) quantification is the common procedure used for the diagnosis of AMI. It is also being used for early rule-out when using high sensitivity (hs) assays, which improves risk stratification and outcomes assessment in patients presenting with ACS and non-ACS myocardial injury. The ongoing use troponin quantification has made it a potential candidate for AMI prevention[7,8]. Troponin assays have rapidly replaced creatine kinase assays because of troponin myocardial tissue specificity[9,10]. The European Society of Cardiology and the

American College of Cardiology (ESC/ACC) redefined AMI as troponin rise over the 99th percentile with clinical symptoms or electrocardiographic changes indicative of ischemia or coronary artery intervention[11]. The first goal for healthcare professionals in management of AMI is to diagnose the condition in a very rapid manner. Currently the process to diagnose a heart attack involves 12 leads ECG and blood tests, and takes several hours to days due to the time allocated toward sample delivery, preparation and analysis. The development of biosensors that measures cTn concentrations under 30min will lead to faster diagnosis/turn-around-time (TAT), therefore significantly reducing hospital costs by making patients' triage out of the emergency room more manageable hence contributing to better health care. Lab-on-a-chip based biosensors technology offers an opportunity for point-of-care testing (PoCT), or bedside testing. PoCT is a medical diagnostic test performed at or near the point of care, that is at the time and place of patient care. PoCT devices can be classified in two major categories: small hand-held devices and bench-top devices which are primarily bench laboratory instruments which have been made smaller and more user friendly. Several Troponin PoCTs have been developed over the past 40years using techniques such as optical, electrochemical, colorimetric, surface plasmon resonance, acoustic sensors and more. Clinically acceptable cTnI and cTnT POC devices used to assist in an appropriate diagnosis are required to measure cTnI and cTnT with a coefficient of variation (CV) $\leq$ 20% at the 99th percentile upper reference limit (URL). The ESC/ACC has recommended cardiac troponin cutoffs at the 99th percentile of a reference population with a total assay imprecision of $\leq$ 10%. The 99th percentile cutoff point for cardiac troponin T (cTnT) is at 0.01 ng/mL with 10% coefficient of variance value at the 99th percentile of 0.03 ng/mL. The International Federation of Clinical Chemistry (IFCC)

Committee on the Standardization of Markers of Cardiac Damage (C-SMCD) has shown that no cardiac troponin assay currently meets these criteria. La Roche manufactures Cardiac T Quantitative Cobas device which is reported to have a coefficient of variation less than 9% at 0.1µg/mL with no reported 99th percentile upper reference limit[12–14].

1.2 Dissertation objectives

An immunoassay is a biochemical test that measures the presence, or concentration, of a macromolecule or a small molecule in a solution through the use of an antibody (usually) or an antigen (sometimes). The current turn-around time (TAT) for clinical laboratories for cardiac markers results varies from 60-90min. Recommendations for the optimum TAT for cardiac markers from blood collection to results availability vary from 30-60min with a preference for 30min. The TAT challenge for most laboratories arises from the time needed for sample delivery, time for full clot reaction if serum is used, centrifugation to obtain serum or plasma and the 10 – 20-min assay time required for most automated immunoassay analyzers. The evolution of quantitative point-of-care (POC) assays offers a genuine potential for bedside analysis by removing the need for sample delivery to the lab, offering shorter assay times by making the use of whole blood possible, thus eliminating the time necessary for full clot retraction, and the centrifugation step. A recurring issue for any cardiac troponin assay is the assay's lower limit of detection and total precision. This is especially critical for POC testing for cardiac markers as these attributes may be sacrificed for assay convenience[8]. The ESC/ACC has recommended cardiac troponin cutoffs at the 99th percentile of a reference population with a total assay imprecision of ≤ 10%. The International Federation of Clinical Chemistry (IFCC) Committee on the

Standardization of Markers of Cardiac Damage (C-SMCD) has shown that many cardiac troponin assays currently do not meet these criteria. One of the problems with troponin is that it can often take several hours to accumulate in traceable levels in the blood, meaning patients often undergo at least two blood tests over a few hours to accurately identify a heart attack. An approach that minimizes false positive results due to assay imprecision is to implement a pre-concentration step to ensure a higher cardiac troponin cutoff concentration set at the 10% coefficient of variance (CV).

This project addressed the need for point-of-care sensors (PoCS) that are: capable of rapid 'high-resolution' (10%CV at 1 pg/mL and just below 1 pg/mL detection limit) panel assays in a clinic setting, and readily adaptable to new assays in research labs. We constructed a PoCS platform that could reliably be adapted to become an SPR-biosensor. The sensor platform includes a sensing pad and an in-channel reference pad. This sensing module is set to be coupled with an electrokinetic method in the future in order to isolate and concentrate the target biomarkers based on mobilities in electric fields, dielectrophoresis (DEP) and electrophoretic Capture (EPC). This future goal guided the final prototype design.

1.3 Dissertation Summary

Chapter 2 offers a brief overview of point-of-care devices potential and growth. Chapter 3 presents the different techniques available to quantify troponin along with their detection limits. The principle of surface plasmon resonance and its different applications are described in chapter 4 as well as how SPR inspired the development of the platform to be used for the SPR-biosensor in this dissertation. Chapter 5 details the different steps and techniques used for the fabrication of the SPR platform and its

adaptation into a potential sensor. Chapter 6 offers a survey of the different techniques used to characterize the platform. Chapter 7 goes over a brief sensor performance and the potential application of the developed surface.

Chapter 2

POINT-OF-CARE TESTING

2.1 Market Growth

The availability of point of care testing boomed over the past couple of decades. Due to their convenience of use, their market growth is expected to continue rising. The U.S. Food and Drug Administration defines In Vitro Diagnostics (IVD) as: tests done on samples such as blood or tissue that have been taken from the human body. In vitro diagnostics can detect diseases or other conditions, and can be used to monitor a person's overall health to help cure, treat, or prevent diseases. The point-of-care diagnostics market is projected to grow at a CAGR of 10.0%. The global point-of-care diagnostics market is projected to reach USD 30.13billion by 2022 from USD 23.71 billion in 2017 at a compound annual growth rate (CAGR) of 10.0%[15,16].

2.2 Point-of-Care Testing devices features

POCT devices possess common features that makes their use convenient in the clinical settings for the users. The core features of POC devices are: simple of use, reagents and consumables are robust in usage and storage, results should be in accordance with the established laboratory method and finally device together with associated reagents and consumables are safe to use. Because of the potential of POCs to revolutionize healthcare, by improving diagnosis speed while maintaining the test accuracy, time and cost as have become two key additional features that today guides the design of POC devices[17]. The World Health Organization provided guidelines known as ASSURED for PoCT used for the detection of sexually transmitted infections:

Affordable

Sensitive – minimal false negatives

Specific – minimal false negatives

User-friendly – minimal steps to carry out the steps

Rapid & Robust – short turnaround time and no need for refrigerated storage

Equipment free- no complex equipment

Delivered – to end users

The ASSURED criteria are a benchmark to decide if the tests fulfill disease control needs[18,19].

The difficulty to deliver a device meeting all these requirements inspired Hsieh et al. to conduct a survey to gauge which of the features was the most important to clinicians; as a result, TAT turn out to be the biggest barrier and accuracy the most important feature identified by clinicians and others offering STI services. Hsieh et al. performed another survey, this time for industry professionals and for that group a TAT of 15min was preferred whereas 5min was preferred by the previous group.

2.3 Types of Point-of-Care Testing device

POCs devices can be divided into two groups: group 1 that consist of large bench top devices with complex built in fluidics and group 2 that consists of small hand-held devices including quantitative and qualitative strips. PoCT devices exists in a wide variety for a wide range of application. They convenient size and ease of use makes them easily accessible by the patient themselves within their own home or healthcare professionals at the patient site or bedside. Most of the handheld PoCT uses fingerstick capillary sample collected from the patient to the PoCT device, with minimal to no

sample prep required, device performing the analysis. Dipstick PoCT is one of the oldest commercially available PoCT device. One of its most popular application is urine analysis. The most popular and currently investigated type of PoCT is called immunostrip; antibodies that bind to the analyte is coupled with reflectance or fluorescence spectrophotometry detection. Immunostrip PoCT comes in several different formats and will be discussed in chapter 3 that focuses on the current state of PoCT devices for troponin measurements. Two types of detection system are commonly used in PoCT devices: photometric or electrochemical. Electrochemical detection has made possible the miniaturization of glucose POCT devices and well as the development of a take device for patient self-monitoring. The i-STAT devices perform the analysis of whole blood and has the result delivered directly to the operator; it has the capability to analyze different type analyte (one type of analyte at the time) depending on the cartridge being used. Because of its one protocol that fits all, it allows the operator to only be required to learn one protocol which also cuts down on the use of the devices and possible operational errors[20].

2.4 Emerging technology

Advancement of miniaturization and microfabrication techniques from the microelectronics industry have helped Lab –on-a-chip (LOC), also known as microchip, evolution over the past couple of decades. Such techniques have helped the analysis to be performed on the microscopic scale (1-500um) by making possible the incorporation of micro: filters, channels, arrays, pumps, valves and bioelectronics chips[17]. Silicon, glass or polymer have been used a support for the fabrication of the microchip. The microchip being the core of the analysis, integrates into one reaction cell all the

processes associated with the analysis in question: from sample placement into the chip to the analysis itself[21,22].

Lateral flow strip (LFS) is a simple, fast, and cheap technology capable of detecting multiple analyte of interest within 20 min time frame with a single-step[23,24], thus making it popular in biomedicine, agriculture, food and environmental sciences, and a promising platform for the prognosis of condition such as heart failure[25,26]. LFS technology, popular on the PoCT market, has some limitations that are common to other types of PoCT. One major limitation to small hand held PoCTs is their need for multiplexing, the ability to measure multiple analytes on the same strip. The second major problem for PoCT, including LFS, is their limited sensitivity which has been demonstrated by tuberculosis testing. In order to cut the cost down to make analysis available in developing world, the development of paper based analytical devices came into important consideration. The issue of sample contamination is also to be considered during the design of the device. Several challenges arise when developing a PoCT device ranging from the integration of sample preparation with other analytical sub-processes to deliver a complete analysis without an operator, which will follow the format: sample in – result out. Detection and read-out modality represent another major limitation of PoCTs development[27]. Fluorescence based measurements, absorbance, light scattering and other optical detection methods rely on electrochemical measurements. The translation of the chemical signal to the user could pose an issue if used in remote location. To remedy to this issue, the use of smartphones is being investigated in order to make the interface user friendly. Smartphones, alone or coupled with add-on devices, have been used for data collection, analysis, display, and transmission, establishing their popularity in POC diagnostics. Early POC technologies

usually require extra peripheral devices for analytical evaluation, therefore making the test costlier and more complex and also limiting its mobile application[28].

Chapter 3

STATE-OF-THE-ART MEDICAL MEASURMENT OF CARDIAC TROPONIN

AMI diagnosis is increasingly depending on the quantification of troponin for faster and more accurate diagnosis. Clinical assessment, 12 lead ECG and cardiac troponin quantification form the diagnostic corner stone for AMI patients[8,28,29]. An immunoassay is an analytical technique which uses antibodies for the selective determination of sample components. Immunoassays are commonly used in a wide variety of areas, especially in biochemistry and clinical chemistry. In clinical setting, enzyme-linked immunosorbent assay (ELISA) is a selective method commonly used to monitor troponin concentration. The ELISA assay uses the coupling of antigens and antibodies and relies on the specificity and affinity of antibodies for antigens. ELISA assay can be grouped into four categories: direct, indirect, sandwich, competitive and multiplex ELISA. The sandwich assay or antibody capture assay is the most commonly used. A "sandwich" ELISA is used to detect sample antigen. A surface is prepared to which a known quantity of capture antibody is immobilized resulting in any nonspecific binding sites on the surface being blocked. The antigen sample is then added to the plate, and captured by the previously immobilized antibody. Unbound antigens are removed via a wash step. A second specific antibody is then added, that binds to the antigen, hence the 'sandwich' because the antigen is trapped between two antibodies. This first immobilized antibody, primary antibody, could be in the serum of a donor to be tested for reactivity towards the antigen. The second added antibody, secondary antibody, is conjugated to an enzyme (such as HRP or AP). A substrate for the enzyme conjugated to the antibody is then added, which causes the color change upon reaction with the

enzyme. The higher the concentration of the secondary antibody present in the sample, the stronger the color change. A spectrometer is used to give quantitative values for color strength. Depending on the nature of enzyme on the secondary antibody, after the addition of its substrate, its signal can be converted into a color or fluorescent or electrochemical signal.

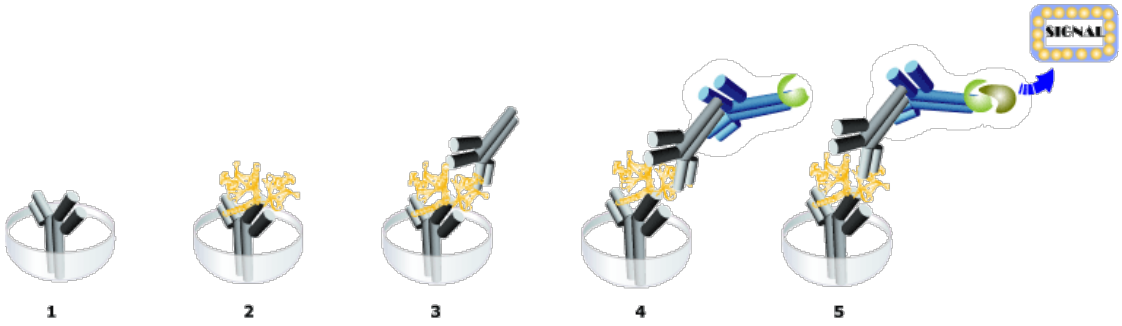

Figure 3.1: (1) Plate is coated with a capture antibody; (2) sample is added and any antigen present binds to capture antibody; (3) detecting antibody is added, and binds to antigen; (4) enzyme-linked secondary antibody is added, and binds to detecting antibody; (5) The second antibodies, which will bind to any antigen-antibody complexes, are added to the wells. These second antibodies are coupled to the substrate-modifying enzyme.[30]

The major drawbacks on the traditional ELISA assay is first, that the assay turnaround time may range from hours to days due to lengthy bio-analytical methodologies and delays in the transportation of samples from the patients to the laboratory which adds on to the lengthy sample preparation, second that the cost is high due to the expensive equipment used for the analysis, the antibody production and the qualified personnel[31,32].

Numerous studies have generated more sensitive and specific diagnostics for troponin. Point of care testing (PoCT) provides an opportunity for rapid diagnostics assay to be

performed at the patient' site, immediately improving TAT. More effective medical interventions will be enabled through personalized diagnoses by improving POCs sensitivities to pg/mL for determining protein biomarkers in whole blood. Several novel techniques used to quantify troponin are minimally invasive and have lower limits of detection. Four major techniques used have been investigated over the past 40 years to develop faster and highly sensitive troponin biosensors for more accurate diagnosis:

- Acoustic biosensors
- Electrochemical biosensors
- Paramagnetic biosensors
- Optical biosensors

3.1 Colorimetric assay

Colorimetric assays are designed to help quantify a particular analyte in an assay by measuring the amount of photon absorbed by the reagent or the chromogenic reaction in the presence of the analyte of interest produced at a characteristic wavelength, with the wavelength being specific to the analyte being analyzed. The greater the analyte concentration, the greater the light will be absorbed. A very common colorimetric assay used to quantify troponin is ELISA. In ELISA sandwiched assay, the principle is such that that the antigen (Ag) is captured in between two antibodies Ab1 and Ab2. Ab1 is immobilized at the bottom of the plate and first captures Ag. Ab2 is linked to an enzyme that will be added to the Ab1-Ag complex to form a sandwich. The final change of color is proportional to the analyte concentration. HRP is the enzyme often conjugated to the secondary antibody, which can initiate a chemiluminometric signal that can be exploited to build a colorimetric assay.

Cho et al. successfully developed an ELISA-on-a-chip (EOC) biosensor for cTnI. The sensor was built using a cross-flow chromatography also known as cross flow filtration, vertical channel for holding the immune-strip, and horizontal channel to allow the detection of variable signals from the complex formation sites. They functionalized the sensor's surface with BD clone 12 (BDc12), a monoclonal antibody specific to cTnI, via biotinylation which is the process of covalently attaching biotin to a protein, nucleic acid or other molecule. A secondary BDc 12 was labeled with HRP to generate the chemiluminometric signal to be captured by the detector. Once the analyte, cTnI, was successfully sandwiched between primary and secondary BDc12 antibodies, HRP substrate luminol was passed through the immobilized surface to generate a chemiluminometric signal proportional to the cTnI surface concentration. After primary BDc12 have been immobilized onto the surface, the TAT from analyte incubation to measurement process was approximately 20min. Cho et al. reported their EOC biosensor system was capable of detecting cTnI present in serum at concentrations as low as 0.027 ng/mL[33].

Gold nanoparticles (AuNP) based colorimetric assay have shown success in the development of cTnI sensors. Wu et al. conveniently engineered a PDMS-gold nanoparticles composite film-based biosensor; the sensor surface with troponin and troponin antibodies was analyzed. The amount of silver reduced correlates to how much troponin was bonded to the antibodies. This method reported measurement of 0.01ng/mL, but an incubation time of more than 1h after antigen addition decreases it potential use as a PoCT[34].

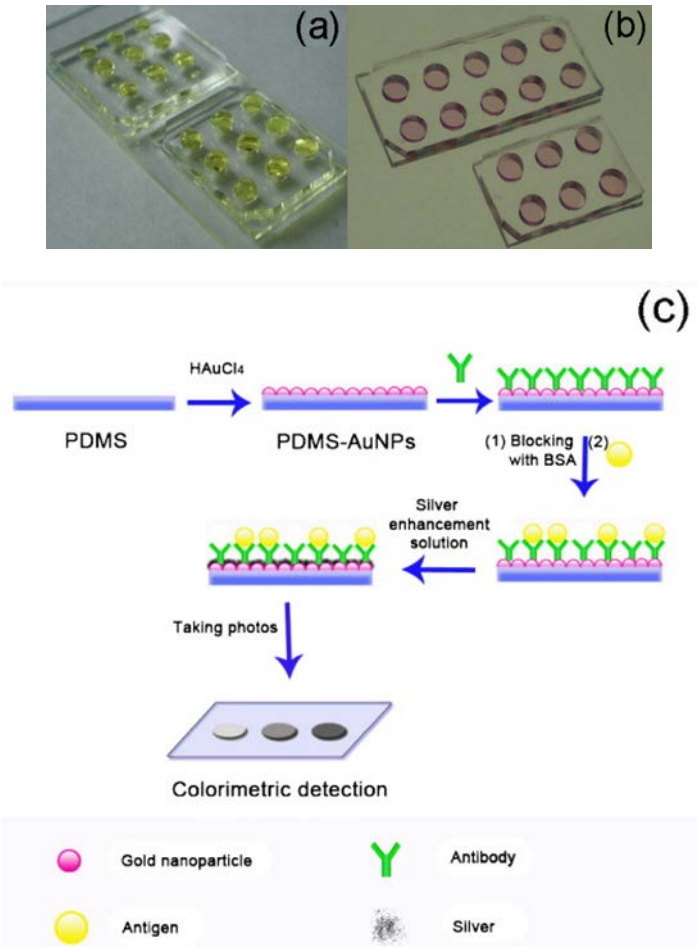

Figure 3.2: Experimental procedure for silver enhancement colorimetric detection of cardiac troponin I; (a) is the PDMS chip with HAuCl4 solution; (b) is the photo of PDMS-AuNPs composite film; (c) schematic diagram for colorimetric detection.[34]

3.2 Fluorescence assay

Florescence immunoassay, another form of optical biosensor, represents the biggest group of currently used and commercially available biosensors. The first fluorescence immunoassay can be dated as far back as 1941 by Coons et al.[35]. Fluorescence organic dye and fluorescent nanoparticles are mainly used as signal molecules to track the analyte of interest. It has been popular among commercially

available sensors because of their fast TAT. Alere, bio Merieux, Siemens, Response Biomedical, Cardiac Reader and more have reported an analytical time within 20min. Wu et al. examined the analytical performance of the ZeptX™ System (Singulex) assay for cardiac troponin I (cTnI). They reviewed its sensitivity, precision, and recovery. High sensitivity with detection limit of 1.7 ng/L cTnI concentration was achieved, and the data obtained demonstrated the presence of AMI earlier than a traditional cTnI assay. The main drawback of the modified ZeptX is that measurement these systems requires high initial and high maintenance costs[36].

Table 3.1: Analytical Characteristics of Commercial Cardiac Troponin I Assays Declared by the Manufacturer[37]

Device	LOD (µg/L)	99th % (µg/L)	Detection Tag
Abbott i-STAT	0.02	0.08	ALP
Radiometer AQT90 FLEX TnI	0.0095	0.023	Europium
Alere Triage Cardio 3	0.01	0.02	Fluorophor
Roche E 2010/602 cTnI	0.016	0.16	Ruthenium
Siemens Dimension EXL TNI	0.017	0.056	Chemiluminescence
Siemens IMMULITE RxL CTNI	-	0.07	ALP
Tosoh ST AIA-PACK	-	0.06	ALP

3.3 Paramagnetic assay

Paramagnetic particles (PMPs) use in assay emerged in the 1970s. They have been applied in several fields such as: MRI contrast agents and biomolecule separation. PMPs usually consist of an iron oxide core with a biocompatible outer layer. Most PMPs based immunoassay follows the antigen-antibody sandwich assay format that is immobilized on the surface with PMPs, serving the purpose of labels[38–41]..

Bruls et al. used troponin antibodies coated PMPs to fabricate a multiplexed cTnI immunoassay. The coated PMPs were mixed with a cTnI sample and allowed to interact. During that interaction, the troponin is sandwiched in between the antibodies on the bottom surface and the antibody on the PMPs. Once the antigen-antibody interaction time is complete, a magnetic field is used to remove the non-bonded PMPs (Figure 3.4). The concentration of cTnI is proportional to the amount of PMPs, therefore the amount of light reflected from the surface is indicative of the cTnI concentration. The measurements are done using frustrated total internal reflection (F-TIR). The combination of optical and magnetic technique was able to generate a detection limit of 0.03ng/mL[42].

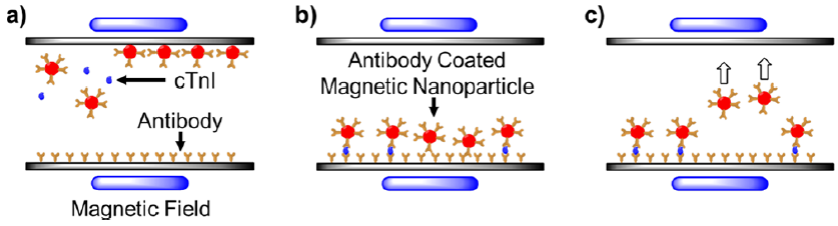

Figure 3.3: a) cTnI and antibody coated magnetic nanoparticles were mixed in the channel. (b) cTnI were captured by the antibody on the bottom surface, also sandwiched by the antibody coated magnetic nanoparticle. (c) Unbound particles were washed away by the upper[42]

Unlike Bruls et al. immunoassay based sensor, Kiely et al. sensor does not need the extra washing step. This is made possible because the PMPs present in the sample cause the coil's inductance to increase which leads to direct determination using a bridge circuit. The sensor's assembly is composed of a detection coil and a reference coil. The PMPs detection was done using a sandwiched format assay; troponin antibodies were immobilized on the detection coil and the PMPs which will allow the troponin to be captured in between the antibodies once added to the device. The whole process is completed within 4min and offers measurements as low as 0.5ng/mL[43].

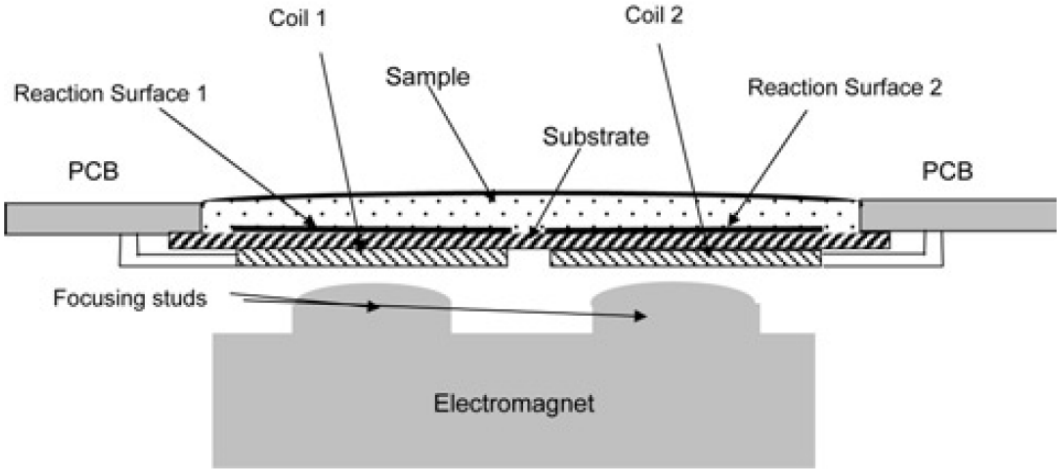

Figure 3.4: Schematic of the biosensor showing the reaction surfaces at the base of the vessel and the corresponding detector coils[43]

The Erenna, immunoassay system originally developed by Singulex® which uses Ultrasensitive Single Molecule Counting (SMC™) technology, was used by Todd et al. to combine paramagnetic and optical immunoassay. They reported a LOD of 0.6ng/mL with a dynamic range of >435 logs. Coated magnetic particles (MPs) were incubated in antibodies coated 96-well plate. Once the incubation time completed, unbounded MPs

are removed using a magnetic bed. Once unbounded MPs are removed, urea is used to disrupt the antibody-analyte interactions to release cTnI from the MPs then pumped into the Erenna immunoassay system. The freed fluorescent labeled cTnI solution is passed through an interrogation space. The light generated from a laser is directed via a dichroic mirror and a confocal microscope lens into the interrogation space which then interacts with dye-labeled antibodies as it passes through this space. The dye-labeled antibodies emit fluorescent light, which is measured via the confocal microscope lens and a photon detector. The output from the detector is a train of pulses, with each pulse representing one detected photon[44].

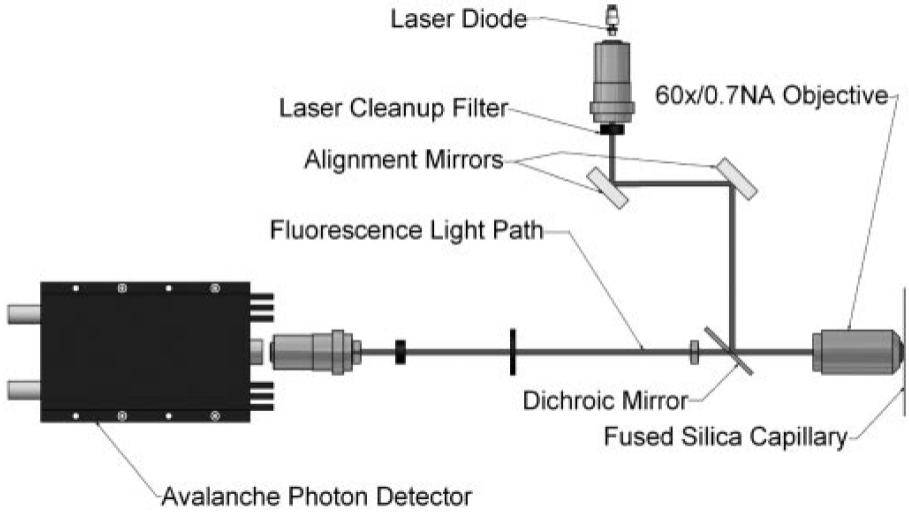

Figure 3.5: Schematic representation of the Erenna Immunoassay System[44]

3.4 Acoustic biosensors

Unlike common biosensors platforms that require the use labels, such as fluorophores and radiolabels, acoustic-based sensors work on the principle of using a piezoelectric crystal change in frequency caused by the mass accumulation on its

surface. Similar to Surface Plasmon Resonance (SPR), acoustic biosensors eliminate the need for long sample preparation time and additional cost due to the labeling process. The two main type of acoustic biosensors are quartz crystal microbalance (QCM) and surface acoustic wave sensors (SAW). As mass accumulate onto QCM crystal surface it causes a change in its resonant frequency. The relationship mass and resonant frequency is translated into the Sauerbrey equation:

$$\Delta f = \frac{-2f^2\Delta m}{A\rho\upsilon} \quad (3.1)$$

where A is the QCM active area in cm2, f is the resonant frequency of the QCM in Hertz, Δm is the change in mass in grams, ρ is the density of the quartz crystal in g/cm3, and υ is the shear wave velocity in the quartz (cm/s)[45].

Wong et al. developed a QCM based sensor for the detection of troponin T and reported a limit of detection of 5ng/mL[46].

A SAW based sensor works on the same principle as a QCM based sensor. The difference comes in the format the signal is monitored. In SAW detection technique, the transducers convert the electrical signal into a polarized transversal acoustic wave which travels across piezoelectric crystal. Once mass accumulated onto the piezoelectric crystal, the original frequency of the acoustic wave is shifted. The shift is proportional to the binding events occurring. Lee et al. developed a rapid and sensitive SAW immunosensor that made use of gold staining as a signal enhancement method. A sandwich immunoassay was used in the sensing area of the SAW sensor dedicated to specifically capture and detect cardiac markers including troponin. The analytes in human serum were captured on gold nanoparticles (AuNPs) that were conjugated in advance with detection antibodies.

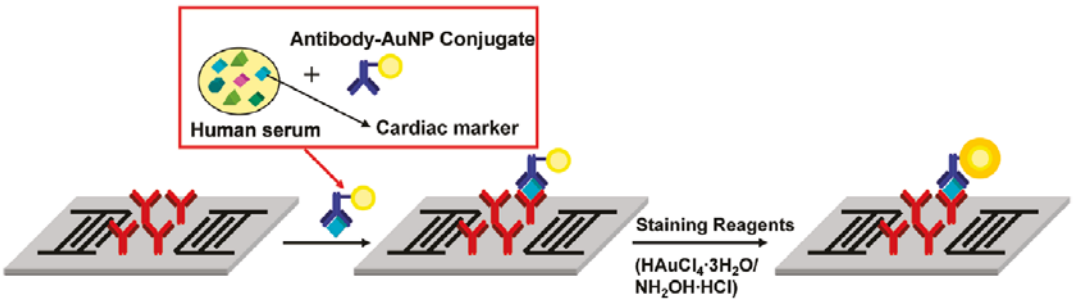

Figure 3.6: Schematic of the sandwich immunoassay format utilized in this study in combination with gold staining[47].

The sensor response indicated that amount of the adsorbed cardiac marker-AuNP complexes was proportional to the applied cardiac marker concentration. They reported a minimum detectable troponin concentration of 20 pg/mL[47].

3.5 Electrochemical assay

Electrochemical assay-based biosensors operate on the principle of change in the current, impedance, or potential difference when immunoreactions take place on the electrode sensing surface. Electrochemical sensors are divided into four main categories: impedimetric, amperometric, potentiometric, and conductance-based sensors. Nanoparticles have been a popular material for the development of electrochemical biosensors, which gave rise to a variety of novel troponin detection platforms. A nitrogen-doped reduced graphene oxide (N-prGO) was used for detecting and quantifying of cTnI by Chekin et al. The N-prGO electrode surface was non-covalently modified by 1-pyrenecarboxylic acid (py-COOH) and poly(ethylene glycol) modified pyrene (py-PEG) ligands which allowed the covalent integration of Tro4 aptamer, needed because of its high selectivity towards cTnI. Differential pulse voltammetry (DPV) was used and a concentration of 1 pg/mL^{-1} for cTnI was achieved[48]. Ahmad et al. used an indium tin oxide surface that they modified by depositing AuNPs.

The AuNPs had linkers including cystamine and glutaraldehyde that were chemically attached via self-assembly method and permitted the immobilization of primary troponin antibodies onto the AuNPs-ITO electrode surface. Secondary troponin antibodies were labeled with HRP enzyme and used to catalyze peroxide reduction. Once troponin is sandwiched in between primary and secondary antibodies it forms a nanohybrid structure that can be exploited to quantity the cTnI by measuring the changes in open circuit potential during peroxide electroreduction offering a possible troponin measurement of 1ng/mL[49]. A variation of Ahmad et al. work was presented by Shan et al. who didn't use antibodies but instead used two specific peptides: peptide1 (primary peptide) with a sequence of CFYSHSFHENWPS and peptide2 (secondary peptide) with a sequence of FYSHSFHENWPSK. The secondary peptide was labeled with ruthenium bis (2,2′-bipyridine) (2,2′-bipyridine-4,4′-dicarboxylic acid)-*N*-hydroxysuccinimide ester (Ru(bpy)2(dcbpy)NHS) at NH2- terminal. After depositing the AuNPs onto the gold electrode using electrografting, the primary peptide, just like the primary antibodies, was immobilized onto those AuNPs using thiol-containing cysteine at the end of the peptide1. Once the sensing surface is ready, troponin is allowed to react with peptide1. After TnI is bonded to the primary peptide, the secondary peptide is then incubated. The secondary peptide had the property of an electrogenerated chemiluminescence probe (ECL) which generated a strong ECL signal directly proportional to the logarithm of the concentration of TnI. The measurements reported ranged from 1 to 300pg/mL[50]. Abbott i-STAT, a commercial cardiac troponin I POC device, uses amperometric detection and reported an analysis time under 2min with a limit of detection of 50ng/mL[51].

3.6 Surface plasmon resonance assay

Surface plasmon resonance (SPR) is an exceptional optical technique that measures the change in refractive index adsorption. SPR label free ability enables rapid detection and makes it a strong candidate for PoCT application. Masson et al. investigated to possibility of a fiber optic based SPR sensor, using a direct capture format, for troponin I detection and reported an LOD of 1.4ng/mL[52]. Kwon et al. constructed a troponin I sensor by crosslinking a monoclonal antibody as an epitope peptide on a chemically modified thin gold film. The lower LOD of that sensor was reported to be 68ng/mL. The measured SPR signal intensity was directly proportional to troponin concentration[53]. Pawula et al. developed a SPR biosensor the for the rapid, sensitive and specific detection of cardiac troponin T (cTnT) in serum samples, using both direct and sandwich immunoassay formats. The detection limit (LOD) for the SPR immunosensor in 50% serum was evaluated to be 5 ng/mL^{-1}. Gold nanoparticles conjugated to the anti-cTnT were used for signal enhancement[54].

Chapter 4

SURFACE PLASMON RESONANCE SPECTROSCOPY

4.1 Surface Plasmon Resonance theory

After its first observation by Wood in 1902[55,56], it is in 1968 that Otto and later that year Kretschmann and Raether demonstrated and offered a complete definition of surface plasmon resonance (SPR)[57,58]. A little over a decade passed when Liedberg et al. first demonstrated an application of SPR to the development of sensors to monitor biomolecular interaction[59]. In fall of 1990, Biacore (GE Healthcare) made SPR sensors commercially available for biomolecular interaction applications[60].

Surface plasmons can be regarded as waves that propagate along the surface of a metal dielectric interface but decays exponentially in the direction perpendicular to the interface[61]; it exist at the interface of two materials with dielectric constants of opposite signs such as a conductive material like metal (m) and a dielectric material (dm), where $\varepsilon_m < -\varepsilon_{dm}$ and ε is the complex permittivity of the given material (Figure 4.1). SPR occurs when plane-polarized or p-polarized light, which has a perpendicular component of the electric field that may excite the surface plasmon, hits a thin conducting film under total internal reflection conditions. In our case gold thin film is used as the metal. The incident light wavevector is k_x, and its magnitude is given by:

$$k = \sqrt{k_x^2 + k_y^2 + k_z^2} = n\frac{2\pi}{\lambda} = n\frac{\omega}{c} \qquad (4.1)$$

where λ, c and ω are the wavelength, propagation velocity angular optical frequency of the incident light in vacuum, respectively.

The direction of the incident light is chosen so the $k_z = 0$, and we remain in a two-dimensional system.

From Snell's Law it is established that:

$$n_1 \sin\alpha = n_2 \sin\beta \tag{4.2}$$

equivalent to

$$k_{x_1} = k_{x_2} \equiv k_x \tag{4.3}$$

thus, allowing the expression for the k_y component of the wavevector, perpendicular to the interface (excited by p-polarized light), to be:

$$k_{y_2}^2 = n_1^2 \left(\frac{2\pi}{\lambda}\right)^2 \left(\frac{n_2^2}{n_1^2} - sin^2\alpha\right) \tag{4.4}$$

In the common SPR set up, incident light travels from high refractive index medium to low refractive index medium; thus, at total internal reflection, $\left(\frac{n_2^2}{n_1^2} - sin^2\alpha\right)$ is negative leaving k_y to be purely imaginary. In conclusion:

$$k = k_x \tag{4.5}$$

The direction of k_x is dependent on: (1) the incident angle (θ_{inc}) and (2) the refractive index of the medium through which incident light travels (n_{inc}). Surface plasmon cannot be excited by photons directly hitting the metal surface because of the component of the light wavevector being much smaller than the propagation constant of the surface plasmon. Therefore, from equation (4.1) and (4.2):

$$k_x = \left(\frac{2\pi}{\lambda}\right) n_{inc} \sin\theta_{inc} \tag{4.6}$$

For the coupling condition to be ideal for SPR, the wavevector of light has to match that of the surface plasmon and it can be done by attenuated total reflection (ATR) or diffraction, therefore:

$$k_{sp} = k_x \tag{4.7}$$

$$k_{sp} = \frac{2\pi}{\lambda}\sqrt{\frac{\varepsilon_{dm}\varepsilon_m}{\varepsilon_{dm}+\varepsilon_m}} \tag{4.8}$$

where λ is the wavelength of the incident light, and ε_m and ε_{dm} are the complex permittivity of the metal and dielectric material; As per the k_{sp} expression shows, the coupling condition are dependent on both the metal and the dielectric permittivity, consequently the coupling conditions change with a change in dielectric material or sample refractive index. As the refractive of the dielectric changes, the coupling conditions in order for k_x to equal k_{sp}.

These coupling conditions are made possible using couplers or coupling devices such as prism, waveguide, gratings.

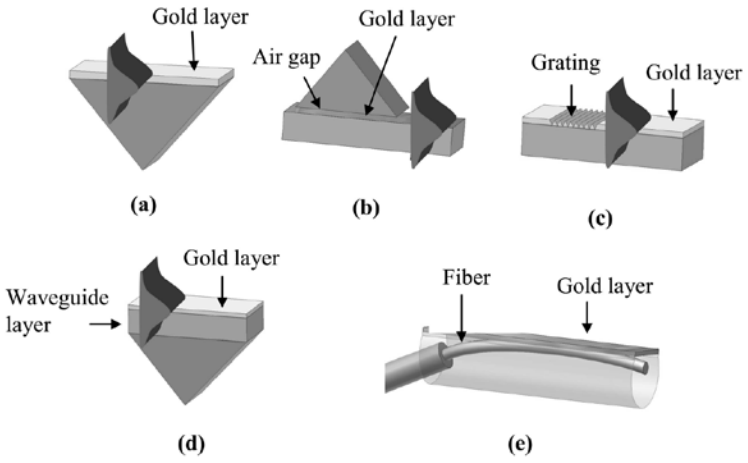

Figure 4.1: Schematics of (a) the Kretschmann configuration of a prism coupler, (b) the Otto configuration of a prism coupler, (c) grating coupler, (d) waveguide coupler, and (e) fiber-optic coupler[62].

Prims are the most commonly used coupling devices, and they are often used in the Kretschmann configuration[63,64].

4.2 The Kretschmann Configuration

The Kretschmann configuration uses total attenuated reflection. This configuration is the most popular in a wide variety of SPR applications and it is set up such that the metal film is placed at the interface of two dielectric media. When the light travels from the higher refractive index of medium 1 to the lower refractive of index medium 2, the total internal reflection (TIR) can take place within medium 1 as long as the incident angle, θ, is greater than the critical angle, θ_c, where $\sin(\theta_c) = n_2/n_1$. The evanescent waves are formed in medium 2 under the condition of TIR. The amplitude of the wave decays exponentially with the distance to the interface of the media 1 and 2. The Kretschmann configuration is the most commonly used set up for generating surface plasmons. In this project the dove prism was primarily used with a multi-wavelength broadband source. The gold film thickness was approximately 50nm and was deposited on a glass slide. The material of the prism is BK7 which has a refractive index of 1.513[62,63].

4.3 Lab-On-a-Chip SPR Sensors

The International Union of Pure and Applied Chemistry (IUPAC) defines a biosensor as an independently integrated receptor transducer device which is capable of providing selective quantitative or semi-quantitative analytical information using a biological recognition element[65,66]. Biomarkers detection in raw biofluids with ultrahigh sensitivity is very beneficial for numerous important biomedical applications such as early stage disease diagnosis and diagnostic testing using non-invasive bodily fluids

(e.g. sweat, urine, tears)[67]. The point-of-care (POC) devices for measuring cardiac biomarkers are rapidly catching up to laboratory-based methods. The laboratory-based analytical devices are much more sensitive than the POC devices, so are preferentially used for diagnosing heart attack but unfortunately have a very long TAT. SPR as a detection technique has been heavily investigated and exploited in biomedical research. BIAcore (Uppsala, Sweden), now acquired by GE healthcare (Chicago, IL, USA), commercial systems have been well adopted by academic institutions and pharmaceutical companies for the use in drug discovery, antibody characterization, proteomics, immunogenicity, immunogenicity, biotherapeutic development and manufacture, life science research application. SPR biosensors main strength is in their label free, real-time and high-throughput format. SPR biosensing has been implemented onto different type of material such as fiber optics (Figure 4.2). SPR additional pros is it abilities to be used as a detection technique for miniaturized sensors to make them more practical as POC device[68,69].

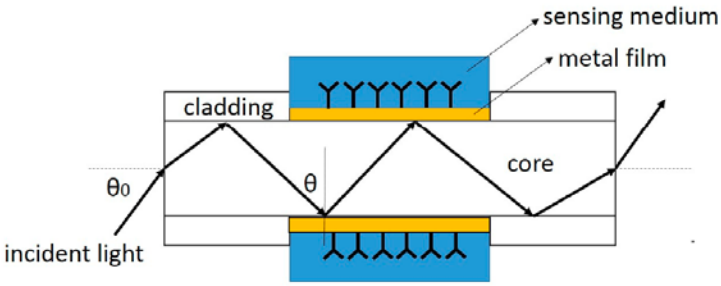

Figure 4.2: Illustrations of a fiber-optic SPR sensor[69] (Missing full stop)

4.3.1 Microfluidics

Microfluidic integration to PoCT devices was necessary for the advancement of biosensors. Common microfluidic devices are based on the continuous flow regimes in micro-sized channels. Droplet-based microfluidic emerged to resolve the issue of sample size, and also create reaction site. First generation droplet-based microfluidic used continuous stream of two or more fluids mainly intersected at a T-junction to create discrete droplets which are isolated from each other using an immiscible fluid (Figure 4.3). The new generation of microfluidic called digital microfluidic (DMF) was introduced in early 2000s, it was an optimization of the previous model by offering a smaller sample size. DMF creates droplets on an array of electrostatically actuated electrodes. Electrowetting-on-dielectric (EWOD) technique is based on changing the interfacial properties of the liquid using an electric field.

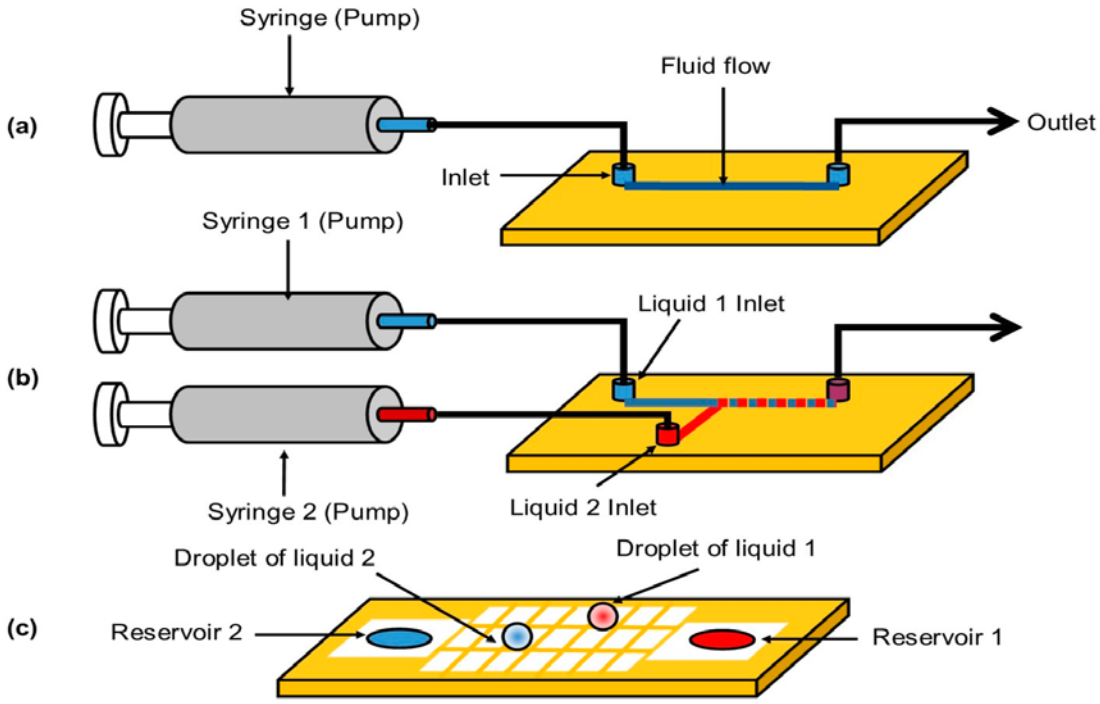

Figure 4.3: Schematic of the three microfluidic systems (a) continuous; (b) drop-based[65].

Microfluidics platform design for biosensors take under consideration dimensions, materials, the method used for fabrication to ensure functionality of the device such as: biocompatibility and wettability of the fabricated device. Even though glass and silicon are the most popular and commonly used in microfluidic platforms, polymer material are gaining a massive interest because they offer lower cost of fabrication and ease in designing. Polymethylmetacrylate (PMMA) and polydimethoxylsiloxane (PDMS) possess great chemical, physical and mechanical properties which also offer great biocompatibility which makes them ideal for microfluidic devices[70].

4.3.2 Electrokinetic sample preconcentration

To improve the TAT of point of care testing, the device used must be set up for sample (eg. Blood, urine etc) analysis with minimal to no sample preparation. Biomarkers are commonly present in low concentration (trace amounts) with a complex matrix (e.g. blood, urine) therefore requiring a preconcentration step that would improve their detection. An electrokinetic method would be a great addition to a microfluidic platform to develop a biosensor with a good sensitivity and an achievable detection limit. In this project we plan to incorporated electrokinetic onto the SPR platform. Dr Hayes and his research team, from the university of Arizona, worked on electrophoretic exclusion method; their work inspired our platform's design.

As stated by Meighan et al., electrophoretic exclusion is a technique capable of differentiation and concentration of proteins in bulk solution[71]. In this method, a hydrodynamic flow is countered by the electrophoretic velocity to prevent a species from entering into a channel. The separation can be controlled by changing the flow rate or applied electric potential in order to exclude a certain species selectively while allowing others to pass through the capillary. A proof of concept was provided using negatively charged polystyrene microspheres and positively charged rhodamine 123 in aspartic acid buffer at pH 2.95. The bulk flow was from left to right, and when potential was applied, the electrophoretic velocity of the dye and the particles was opposing the hydrodynamic flow [72].

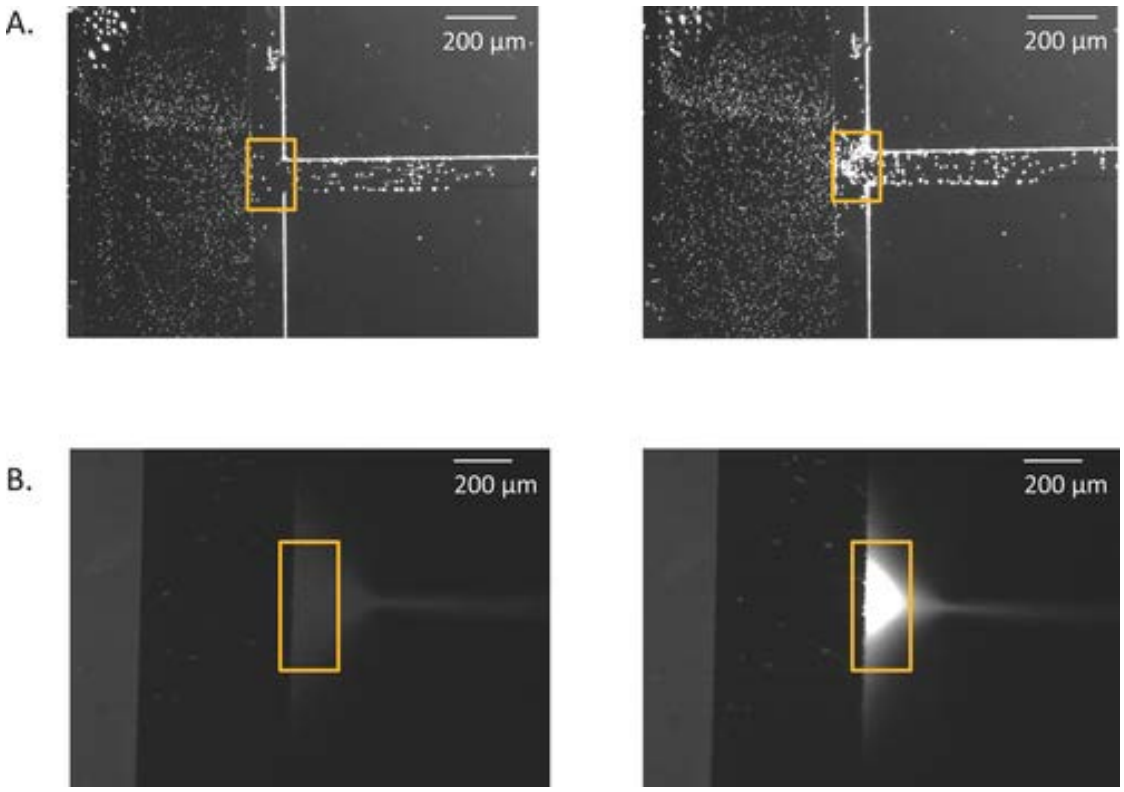

Figure 4.4: (A) Exclusion of beads and (B) rhodamine 123 from a channel entrance. In both cases, hydrodynamic flow is from left to right. Before the application of an electric field, the spheres (A, left) and dye (B, left) travel with the hydrodynamic flow through the system. Once an electric field is induced, the beads (A, right, 300 V/cm) and dye (B, right, −300 V/cm) are excluded in the reservoir near the channel entrance[72].

Figure 4.5 and Figure 4.6 depicts the electrophoretic exclusion process in a channel. The channel was originally filled with two species with differing electrophoretic mobilities in buffer; the white circles represents species with lower electrophoretic mobility than those in black circles. All species are left to move freely through the channels with the hydrodynamic flow in (a). In (b) a large enough electric field is then applied across the

length of the channel to exclude the black circles, that have larger electrophoretic mobility. While the black species are prevented from entering the channel and are excluded within the reservoir, the white species are continuing to flow through the se channel because of their lower electrophoretic mobility. The electrophoretic velocity created by the electric field within the channel counteracts forces of hydrodynamic flow or bulk flow, resulting in the exclusion of the black circles. Once the electric field is removed in (c), all species resume their free flow through the system[71,72]

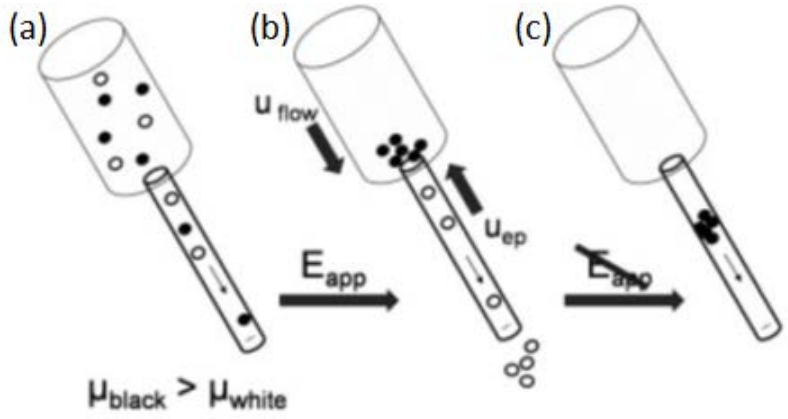

Figure 4.5: Schematic of the electrophoretic exclusion effect. (a) represents the system with no electric field present. (b) demonstrates the exclusion effect when the potential is applied. Because the dark circles have a larger electrophoretic mobility, their movement is arrested at the entrance of the capillary, whereas the lighter species is relatively unaffected by the introduced force. The vial on the right shows the release of the collected[71]

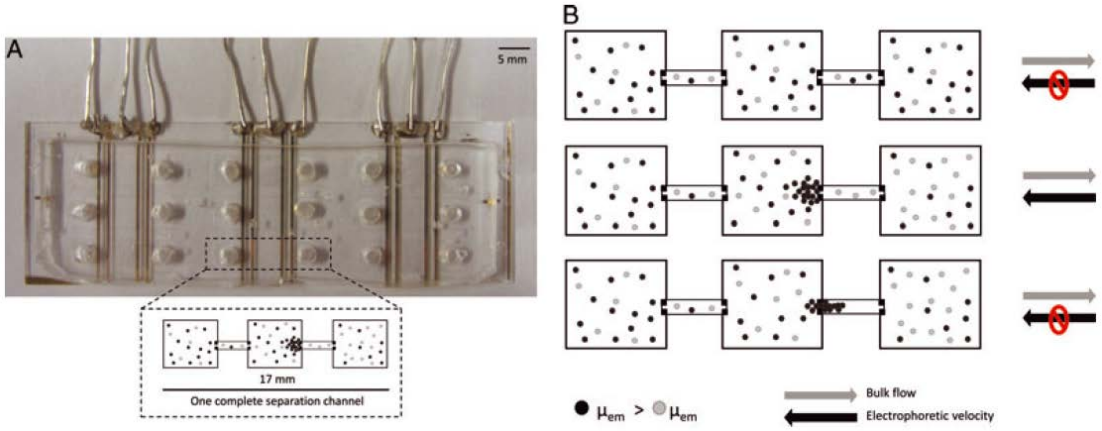

Figure 4.6: Device used for electrophoretic exclusion and schematic demonstrating exclusion principles. (A) A photograph of the complete hybrid glass/PDMS chip with nine separation channels and a schematic of a single channel. (B) A schematic demonstrating the principles of exclusion[72].

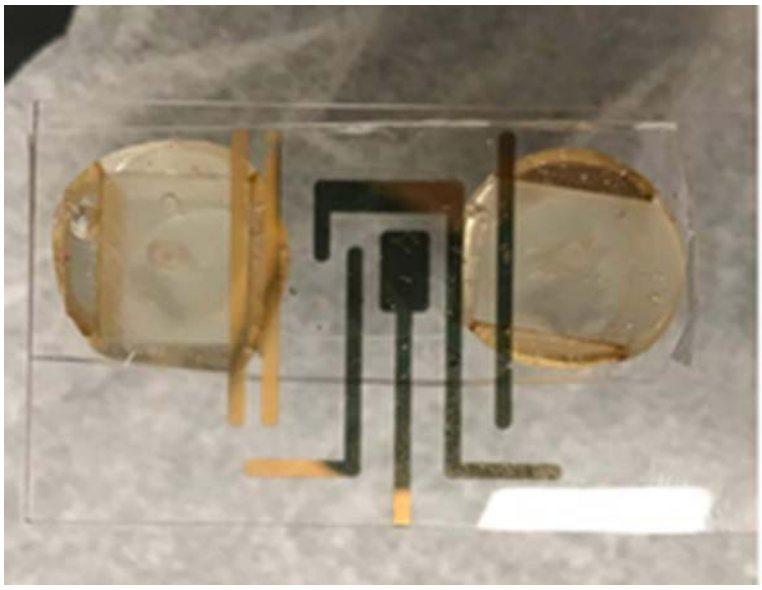

Figure 4.7: Booksh Lab EK-SPR platform

Hayes' group was also able to preconcentrate myoglobin up to 1200 times the background concentration in 60 s. Myoglobin was successfully separated from a solution containing allophycocyanin; both species were negatively charged[73].

As mentioned previously, troponin can take several hours to accumulate in traceable levels in the blood, resulting is a lengthy diagnosis for AMI. The platform designed was inspired by Hayes group platform for electrophoretic exclusion. Our platform includes 4 parallel electrodes to allow preconcentration surrounding the SPR pad to allow the protein preconcentrated prior its diffusion onto the SPR pad.

4.3.3 Conclusion

In this study we present a microfluidic surface plasmon resonance platform that includes an in-channel referencing SPR pad. The platform consists of a 3-electrodes system and is designed to use a PDMS flow-cell. It showed potential to be adapted towards point-of-care testing as a lab-on-a-chip device. We also presented an additional SPR platform with a electrophoretic exclusion set up. Surface plasmon resonance has been used in a variety of industries: food, environmental, clinical. The reference analytical pad within the analysis chamber platform developed, offers the possibility to monitor events with the analysis chamber. Two main issues limiting SPR bioanalysis to be addressed are fouling of the sensor surface and temperature fluctuations.

Chapter 5

METHODOLOGY

5.1 Instrumentation

SPR spectra were acquired with an Andor Technology (South Windsor, CT) Shamrock 303 imaging spectrometer, utilizing a TE-cooled CCD camera also manufactured by Andor Technology, with a rotating grating assembly composed of three different gratings: 150l/mm, 1200l/mm and 1800l/HOLO. The gratings 150l/mm and 1200l/mm were used. In a Kretschmann configuration, light from a white light emitting diode (LED) source was collimated using a collimating lens, passed through a spatial filter (two 10x microscope objectives separated by a pinhole), a polarizer, and a BK7 dove prism used as the coupler for the SPR sensor before entering the detector with a 10μm slit. The sensor made contact with the prism through the use of refractive index (RI) matching oil (RI=1.52). The sensor was connected to a Bioanalytical Systems potentiostat (West Lafayette, IN) using copper wires and alligator clips. The copper wires were used as an extension of the CE, RE and WE to facilitate their connection to the potentiostat.

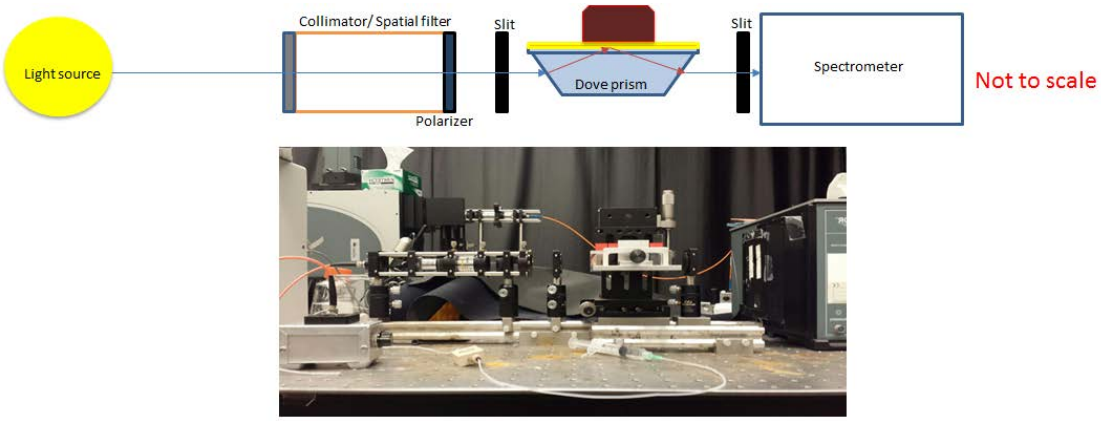

Figure 5.1: Homemade SPR set up

5.2 Additive manufacturing: 3D printing

Additive manufacturing is a term used for rapid prototyping and what is commonly called 3D Printing. The term rapid prototyping (RP) is used in several industries to describe a process for rapidly creating a system or part representation before its final creation is released or commercialized. RP has also been widely used to describe physical prototypes created from a digital model data; the simple principle of this technology is that a model generated using a three-dimensional Computer-Aided Design (3D CAD) system, can be fabricated directly without the need for process planning. 3D printing involves different steps: CAD, conversion to STL, file transfer to machine, machine set up, build, remove, post-process, application.

All 3D printing must start from a software model that completely describes the item in question. Once the item of interest is created in a CAD software, the file is then converted into an STL file format which is then sent for printing. After the file is successfully sent to the printing machine, finale manipulation of the file is performed to ensure the size, the position, and the orientation are correct prior to printing. The 3D printer building parameters, such as materials, energy source, layer thickness and more,

are then confirmed and must be properly before the printing starts. Once the printing started, little to no supervision is required[74].

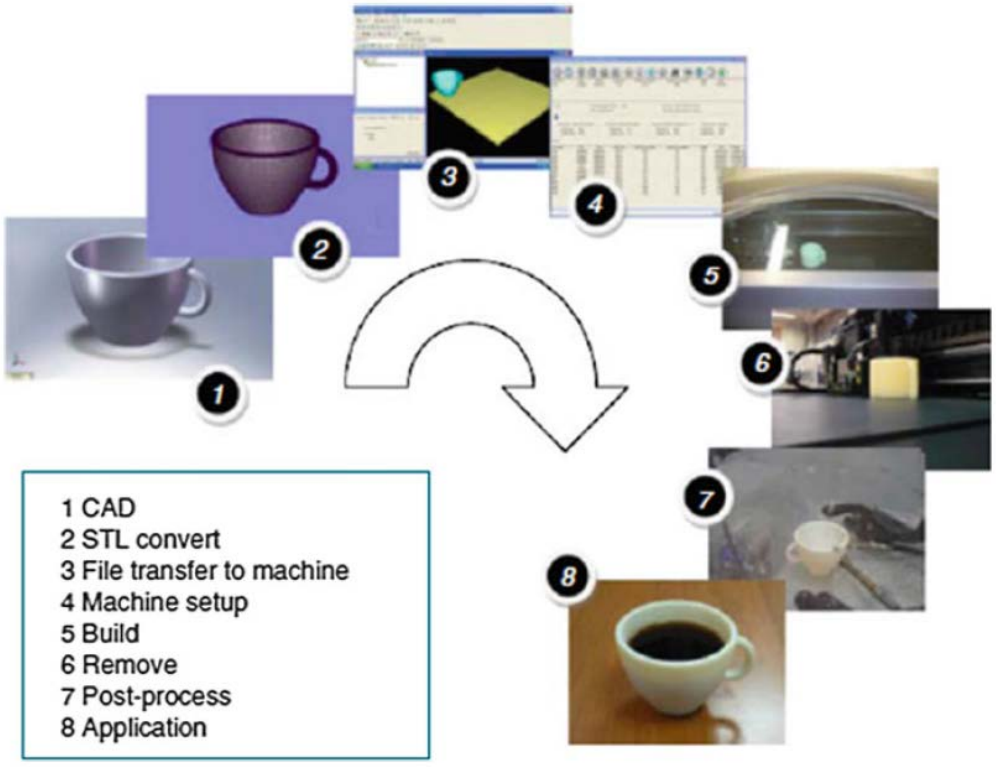

Figure 5.2: Generic process of CAD to part, showing all eight stages[74].

5.3 Mask Fabrication parameters

With a resolution capability of 100 microns and a 410-cubic-inch build volume, the MakerBot Replicator 2 Desktop 3D Printer was the easiest, fastest, and most affordable tool available for making shadow mask templates and photomasks. The software used to create the print file from a computer designed 3D object is MakerBot's own MakerBot Desktop 3.10.0.1364.

5.3.1 Shadow mask Fabrication

A shadow mask is a relatively thin micro-machined metallic template used for the patterning of a substrate. Also called the stencil method, it allows the selective modification of chosen surface area on the substrate. In selective deposition for example a stencil can be used instead of photoresist. Despite the higher resolution offered by photoresist, shadow mask allows faster processing by eliminating several steps such as resist deposition, spin, bake, exposure time, developing photoresist strip and substrate cleaning. Shadow mask are ideal for low resolution processes where alignment to previous layers is not critical.

The shadow masks used in this dissertation work were designed using Tinkercad (Autodesk, Inc., https://www.tinkercad.com/) then the STL file was imported into solid works for the final design. The masks were fabricated at the University of Delaware Machine shop by Mark Schrader. The masks were made of Zinc-Galvanized Low-Carbon Steel Sheet, 0.30mm thick purchased from AK Steel (West Chester, Ohio).

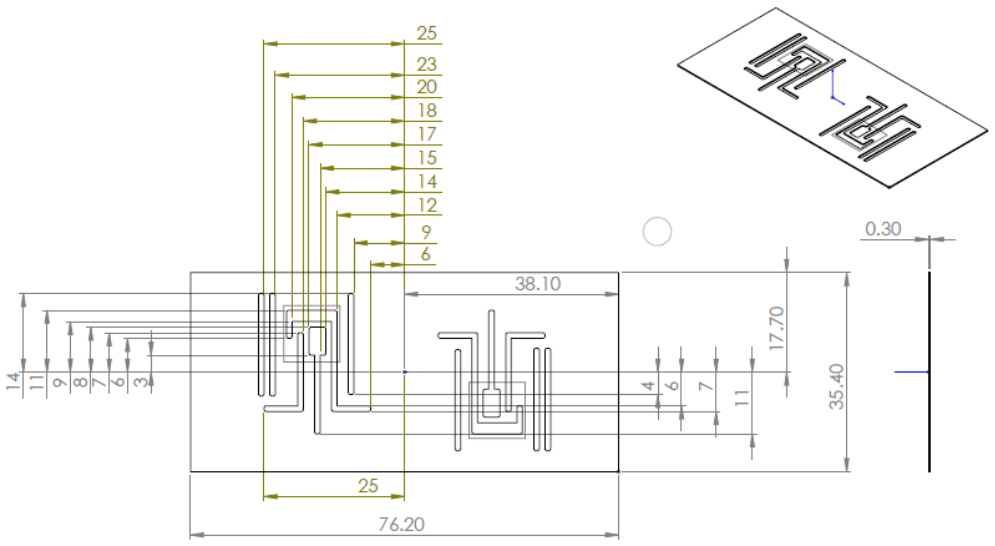

Figure 5.3: Platform-1 deposition mask. All annotated measurements units are millimeters

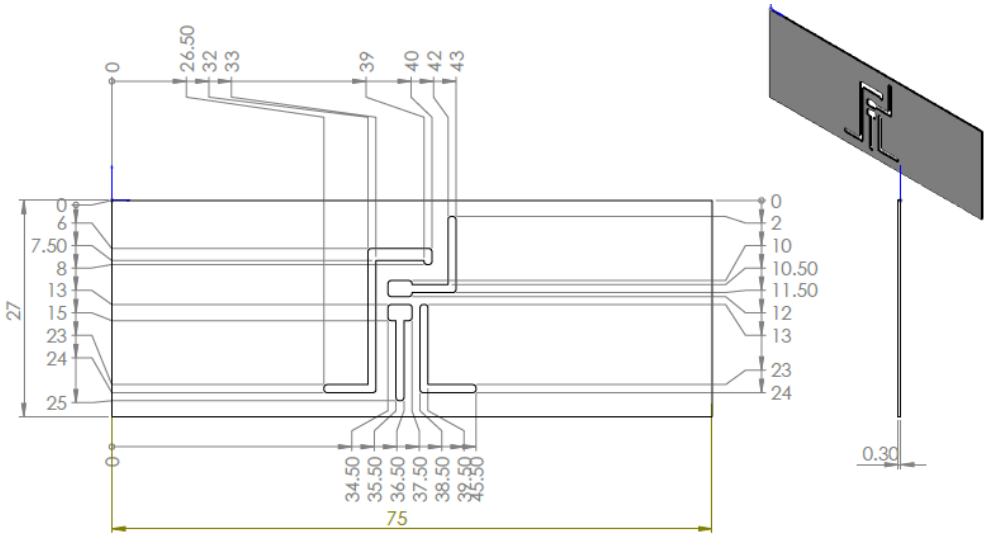

Figure 5.4: Platform-2 deposition mask. All annotated measurements units are millimeters.

5.3.2 Photomask: 3D printer

A photomask is an opaque material (glass or metal or transparencies or polylactic acid) with openings (holes or transparencies) that allows the light to travel through in a predesigned pattern.

The photomask was designed in Tinkercad, exported as an STL file and printed at the University of Delaware Computing Support office by Rick Bernard using 3D desktop printer MakerBot Replicator 2 (MakerBot, Brooklyn, NY) and polylactic acid. The photomask has a diameter of 100mm and a thickness of 2mm. The mask channel pattern was made of 3 squares measuring 10mm each and connected by 2mm channels. The mask was finally painted with black acrylic paint and left to dry to make it completely opaque.

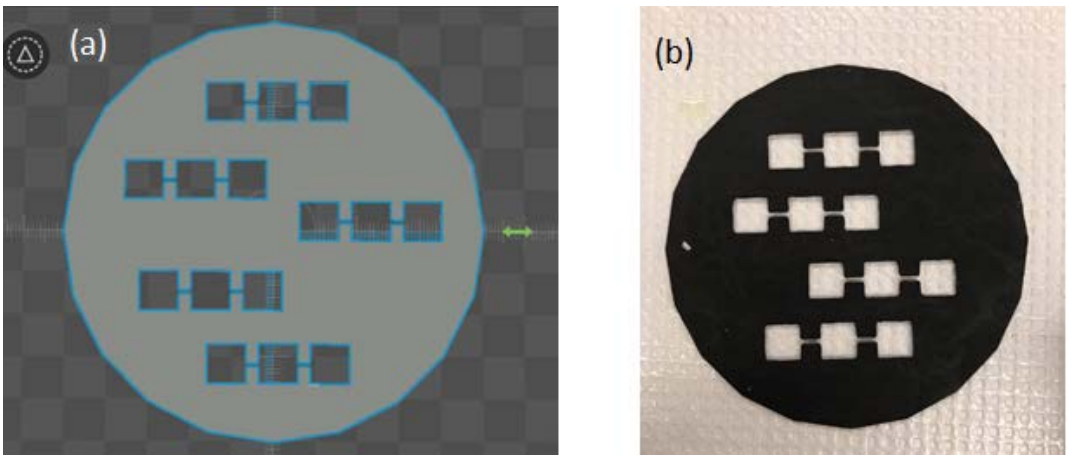

Figure 5.5: PDMS channel photomask (a) STL file, prior printing (b) 3D Printed mask

5.4 Photolithography: Polydimethylsiloxane mold fabrication

A 100mm silicon wafer was coated with negative SU-8 photoresist (MicroChem, Westborough, MA, USA) and developed to create the pattern of the PDMS channels. The wafer was initially cleaned with hot piranha solution [3:1] concentrated sulfuric acid: 30% hydrogen peroxide, both from Fisher Scientific, Pittsburgh, PA for at least 60 min, then abundantly rinsed with deionized water and dried with a nitrogen stream (Grade 4.8, Keen Compressed Gas Co., Wilmington, DE). The wafer was placed in an oven at 105°C to remove water for at least 30 min prior to being coated with photoresist. The recommended coating conditions were used for the mold fabrication. A 5mL syringe was used to dispense Su-8 50 on a static wafer. The photoresist was then spread using a spin coater, from the Surface Analysis Laboratory (LDL 026 University of Delaware, Newark, DE) at a 500rpm speed held for about 10 seconds to ensure the wafer full coverage. Once the wafer was fully covered, the speed was raised to 2000 rpm and held for 30seconds to obtain a thickness of 50µm. After being coated with SU-8 photoresist, the wafer was baked at 65℃ for 6min followed by 20min at 95℃. Once the wafer was cooled, glycerol was placed onto the wafer followed by a clean transparency pressed against the wafer. Additional glycerol is added between the top of the transparency and the bottom of the photomask. Glycerol is used to eliminate as much air as possible at the boundaries of the wafer and transparencies and the photomask. The wafer and 3D printed photomask assembly were set up for UV exposure. The wafer and photomask underwent 3 exposure cycles of 10min and 3 rest cycles of 10mim.alternatively. Once the exposure and rest cycles were completed, the wafer was baked again at 65℃ for 1 min and 95℃ for 5 min. Finally, the wafer was

immersed in SU-8 Developer (MicroChem) and sonicated for 5 minutes until unpolymerized photoresist was completely removed.

5.5 Polydimethylsiloxane (PDMS) gel preparation

PDMS was prepared by mixing a 10:1 mass ratio of polymer to curing agent (Sylgard184, Dow Corning).15g of the polymer to 1.5g of the curing agent was used vs 10g of the polymer to 1g of the curing agent to give the PDMS channel more rigidity, thus preventing the chambers from collapsing during the experiment. The polymer and curing agent were thoroughly mixed then degassed in a vacuum oven. After the degassing cycle, the PDMS was poured onto the patterned wafer and placed in the oven at 80°C for at least 60min. After the PDMS was removed from the oven, it was left to cool on the counter. Once cooled, a pattern was cut using a razor blade and peeled off the wafer. A leather hole puncher was used to create the hole necessary to place the tubing in the reservoirs.

5.6 Surface Plasmon Resonance Sensor electrodes fabrication

Two sensors design were developed. Both designed platform (Figure 5.6 and Figure 5.7) were built onto a 25.4mm x 76.2mm Fisher Brand microscope slide. They contain a microfluidic network of three squared shaped reservoir measuring 10mm x 10mm and connected by 2-mm channels. The center reservoir holds the gold (Au) working electrode, the silver/silver chloride (Ag/AgCl) pseudo reference electrode and the platinum (Pt) counter electrode. All three metals were deposited via e-beam evaporation. On the platform-1, the gold working electrodes surface area is about $30mm^2$ (3mm x 5mm x 50nm). The reference electrode area present within the flow cell

approximates to 10mm^2 (1mm x 5mm x 150nm), the counter electrode surface area is about 46 mm^2. On the platform-2, the gold working electrodes surface area is about 15mm^2 (3mm x 5mm x 50nm). The reference electrode area present within the flow cell approximates to 10mm^2 (1mm x 5mm x 150nm), the counter electrode surface area is about 36mm^2.The PDMS microfluidic channel are produced using SU-8 photoresist developed onto a 100-mm silicon wafer. This platform has a depth 50µm with a volume of approximatly180µL. The Teflon tubing of the flow cell are used to connect the chip to the syringe pump (Harvard Apparatus, USA) to induce volume flow through the channel network.

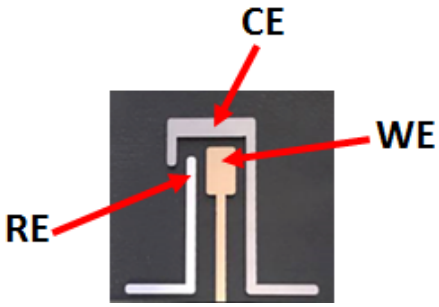

Figure 5.6: EK-SPR-1 3-electrodes system; RE: silver reference electrode, CE: platinum counter electrode, WE: gold working electrode.

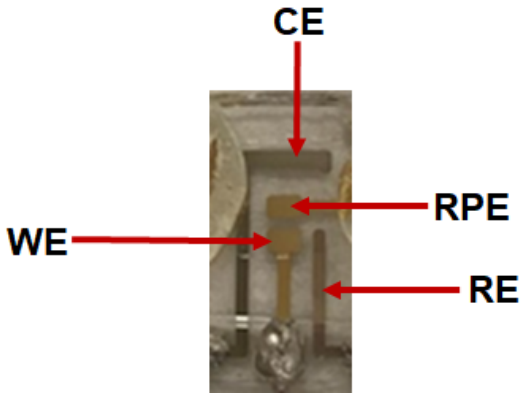

Figure 5.7: EK-SPR-2 3-electrodes system; RE: silver reference electrode, CE: platinum counter electrode, WE: gold working electrode, RPE: gold referencing pad electrode.

5.7 Flow Cell Assembly

The SPR platform was dipped into a 50mM ferric chloride solution for 60s in order to chloronized the silver reference electrode. After the SPR platform was successfully chloronized, a cut-out patterned cured PDMS slab was aligned with the electrodes onto the SPR platform. 6minutes epoxy was used to support Silver epoxy was used to attach and the prepared SPR sensor were placed in an oven for 3 min., followed by the PDMS being placed on the sensor and allowed to self-adhere. The seal was tested by placing water into the reservoir and inspecting for leaks. After successful adhesion, Plexiglas blocks were attached to act as supports for tubing, and leads were attached to the gold electrodes using a conductive silver epoxy. The finished EK-SPR sensor is shown in Figure 5.8.

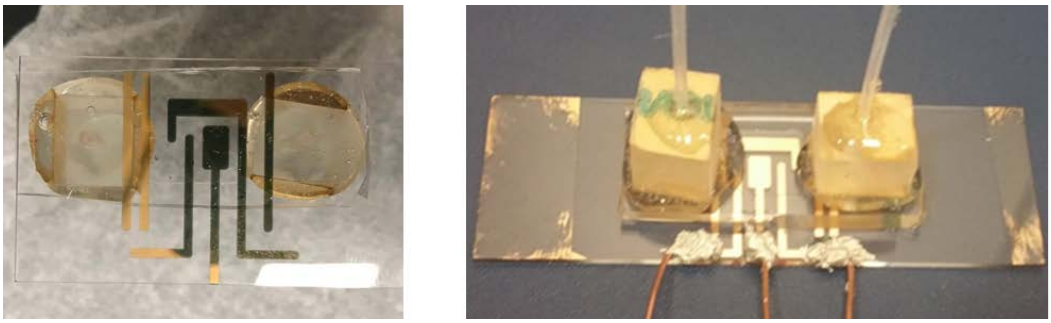

Figure 5.8: EK-SPR flow cell assembled

5.8 Sensor sealing and air bubble removal

The proper sealing of the PDMS flow cell is essential to keep liquid samples in defined volumes, minimize evaporation of samples and reagents from the chip, maintain pressure inside the device and eliminate air bubbles interference during spectrophotometry analysis. The sealing desired for the flow cell developed was accomplished using commercial gorilla glue super glue or All Krazy glue. These liquid adhesives harden by evaporation of their solvent. There was a preference toward the gorilla glue versus the “All Purpose gorilla glue” due to the fact that it was less brittle and offer a rubberier, flexible feels. Two Shut-Off Valve Assembly designed and sold by Index Health Science was used to quickly stops the flow of a stream and help reduce air bubbles. The body of the assembly is made from solvent resistant Tefzel (ETFE) which allows for the use of wide range of chemicals.

Bubble removal was also attempted using technical grade sodium dodecylbenzenesulfonate (SDBS) purchased from Sigma Aldrich (St. Louis, Missouri). SDBS was mixed at different concentration and visually monitored for the removal of air bubbles.

5.9 Surface coating preparation: Diazonium electrografting

The electrochemical platform was composed of three electrodes, consisting of a 50nm gold film sensing working electrode, a 150nm chloronized silver film pseudo reference electrode and a 150nm platinum film counter electrode. The three thin film electrodes were deposited in the University of Delaware Nanofabrication facility clean room using PVD Products (Wilmington, MA) Dual electron beam evaporator. The potentiostat was purchased from Bioanalytical Systems (West Lafayette, IN). Adhesion of each metal film to glass substrate was promoted by performing thorough cleaning of the glass substrates and depositing ~5nm of chromium or titanium as an adhesion layer between glass and each metal film. The glass slides were cleaned in hot piranha solution, a mixture of concentrated sulfuric acid and hydrogen peroxide [3:1], both purchased from Fisher Scientific (Pittsburg, PA) for a minimum time of 60 min, then sonicated 3 times in fresh deionized water and dried with a nitrogen Grade 4.8 purchased from Keen Compressed Gas Co. (Wilmington, DE).The substrates were placed in sterile polystyrene petri dish purchased from Fisher scientific for transport to the University of Delaware nanofabrication facility clean room. Each newly created platform film was stored under vacuum until ready for use.

Thin film electrodes cannot be cleaned or polished using the traditional methods due to their really thin thickness (50-150nm) and could be damaging the silver/silver chloride reference electrode, therefore the most efficient cleaning procedure found was to allow the gold working electrode to undergo potential cycling between −300 mV and +1100 mV (vs. Ag/AgCl thin film) a 10mV/s in 0.5M sulfuric acid until a reproducible cyclic voltammogram was obtained before attempting the electrografting of the diazonium salt. Each electrode was in contact to the potentiostat through copper wires attached using silver epoxy (MG Chemicals, Burlington ON).

The procedure for the preparation of the diazonium salt precursor followed was described by Menegazzo et al. The diazonium salt precursor, 4-amino-DL-phenylalanine hydrate (4-APhe) was purchased from Fisher scientific and dissolved in 0.5 M hydrochloric acid (Fisher Scientific, Pittsburgh, PA) to form a 0.005M solution. The Diazonium salts were generated in situ by adding a 50 µL aliquot of 0.5 M sodium nitrite (99.999%, Alfa Aesar, Ward Hill, MA) to 5.0 mL of the 4-APhe solution and allowed to react for 15 min under 5°C. The reaction between nitrite and hydrochloric acid generates nitrous acid that reacts with the precursor for the formation of the diazonium salt[75].

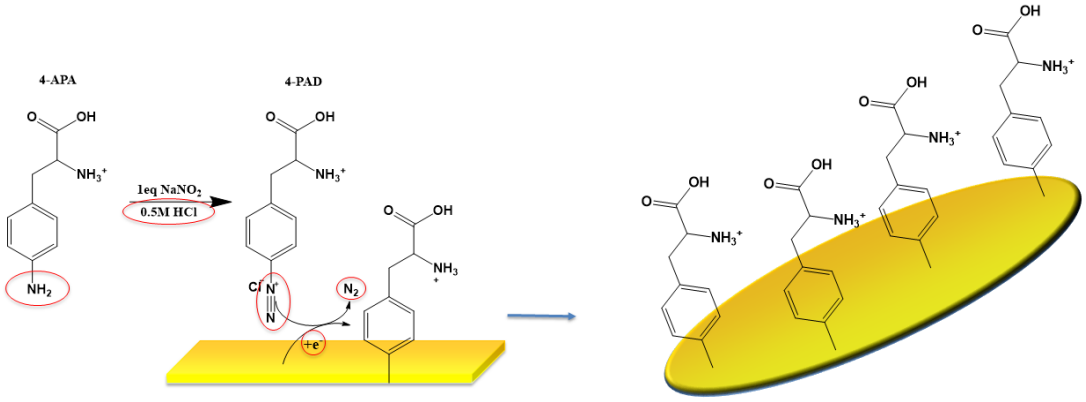

Figure 5.9: 4-amino-L-phenylalanine diazonium salt electrografting mechanism

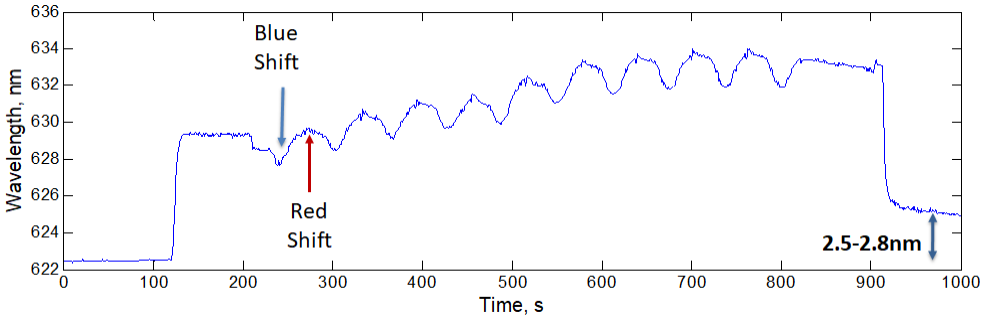

Figure 5.10: Electrografting of 4-amino-L-phenylalanine diazonium progression

Figure 5.9 and 5.10 above, shows the different steps to the electrografting process using cyclic voltammetry. Looking at the provided steps, a ~1.7nm blue shifting occurring at the beginning of every single step can be seen. As the diazonium salt attach to the gold surface, the gold permittivity is modified. The change observed is allegedly representing the change in refractive index at the surface of the gold film. The final shift is the result of the change in the surface refractive index and the bulk. The integrity of the electrodes deposited on the platform were investigated by comparing the cyclic voltammogram of the electrografting using the glass silver/silver chloride reference electrode vs a chloronized silver thin film pseudo-electrode. The results presented in the Figure 5.11 and 5.12 shows that the current difference in between both systems was virtually the same: about $0.5x10^{-4}$A.

a) b)

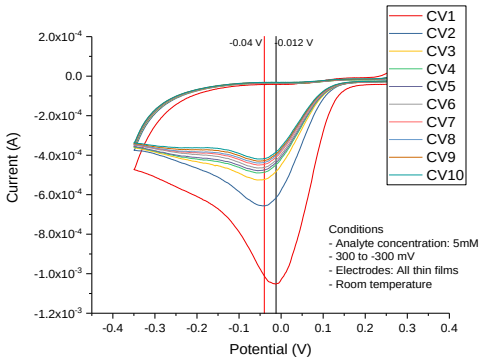

a)

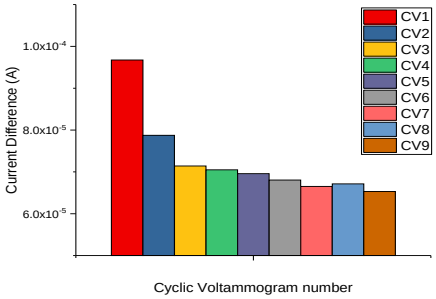

b)

Figure 5.11:4-amino-L-phenylalanine electrodeposition cycling using silver chloronized thin film pseudo reference electrode a) cyclic voltammogram, b) current change over

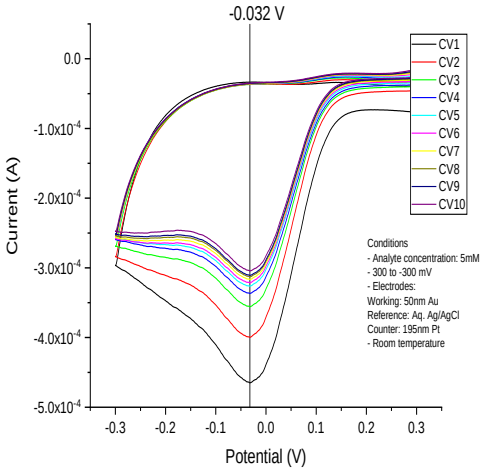

a)

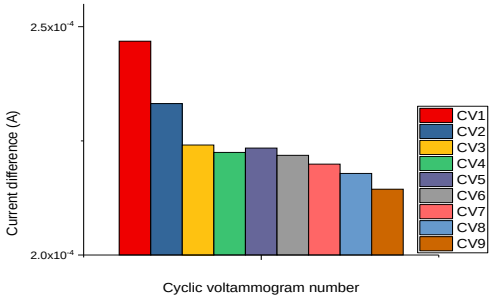

b)

Figure 5.12: 4-amino-L-phenylalanine diazonium electrodeposition cycling using silver/silver chloride reference electrode a) cyclic voltammogram, b) current change over.

Chapter 6

SURFACE CHARACTERIZATION

6.1 Time-of-Flight Secondary Ion Mass Spectrometry (TOF SIMS)

Time-of-flight secondary ion mass spectrometry (TOF-SIMS) was performed in the Surface Analysis Facility at the University of Delaware using a TOF-SIMS IV system (ION-TOF GmbH; Munster Germany). The TOF-SIMS was operated in static mode with a total ion dosage of 1012 ions per cm^2. A bismuth/manganese ion source was used and operated as a high current bunched 25 keV Bi_3^+ mode with a bunch width of approximately 1 ns and ion current of 0.25 pA with a cycle time of 200 μsec. All images where gathered with as 500x500 μm^2 images with 128x128 pixels2 with a beam diameter of approximately 3.6 μm. Typical mass resolution is 6,000 M/ΔM (measured at Si 28 m/z) and all spectra where calibrated to the peaks for H^-, C^-, CH^-, CH_2^-, CH_3^-, C_2^-, C_3^-, C_4^-, C_5^-, C_6^-, C_7^-, C_8^-, Au^-, Au_2^-, Au_3^-, Au_3^-, Au_4^-, and Au_5^- TOF spectra below shows an example spectra of a peak that indicate the bound molecule in this case it is: $Au_2C_6H_4CH_2CHNH_2CO_2H^-$ or $Au_2C_6H_4C_2H_3NH_2CO_2H^-$ or $Au_2C_8H_7NH_2CO_2H^-$ at 559.02 m/z, from Figure 6.1 we see that the peak is unique and clearly identifiable. This peak is one of many indicators, to map the coverage of the molecule many such peaks were combined. Since the coverage intensity is uniform, the coverage is uniform on the scale of 500x500 μm^2 with pixel size of 3.9x3.9 μm^2.

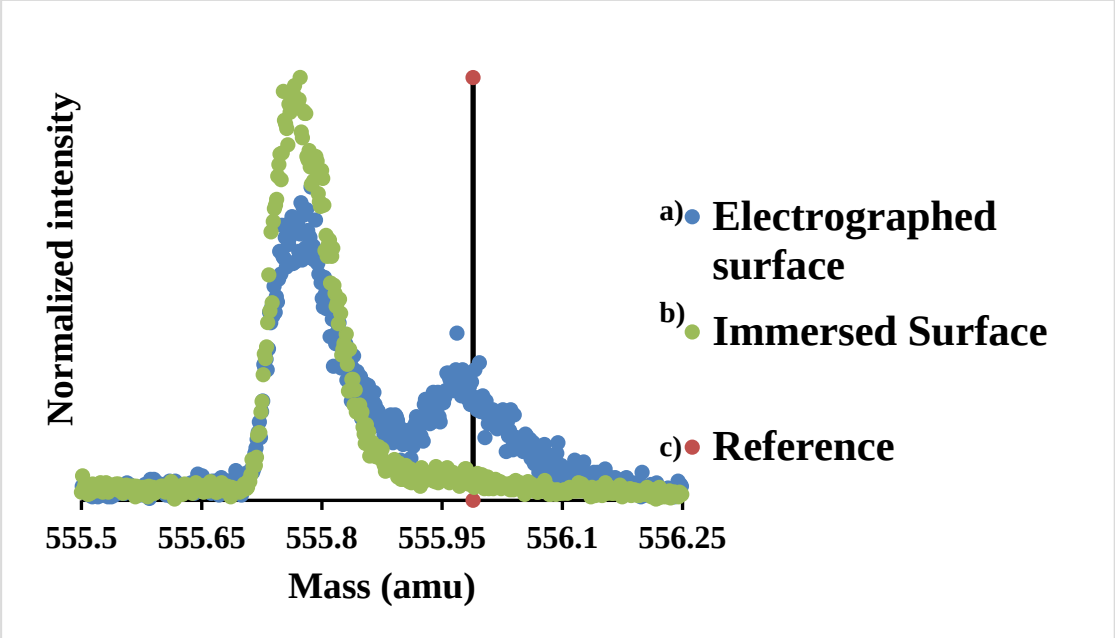

Figure 6.1: TOF-SIMS spectra: a) 4-amino-L-phenylalanine diazonium was electrografted on gold surface, b) gold film was immersed in 4-amino-L-phenylalanine diazonium, c) 4-amino-L-phenylalanine diazonium reference amu.

6.2 X-ray Photoelectron Spectroscopy

XPS was conducted with a K-Alpha+ with MAGCIS (Thermo-Scientific, Inc.) located in the Surface Analysis Facility at the University of Delaware. Monochromated Al Kα x-rays (1486.6 eV) with a spot size of 100 μm was used for all analyses. All high-resolution scans (Au4f, C1s, N1s, and O1s) were run with a pass energy of 20 eV and the scan numbers were adjusted for optimal signal-to-noise ratios. All curve-fitting was done in CasaXPS software using Shirley-type background correction. Figure 6.2 and Figure 6.3 shows carbon XPS survey spectra for an uncoated and a 4-(Phe) modified Au electrode, respectively.

The C1s peak at 284eV is very often used as a charge correction reference because of its high intensity and ubiquitous nature. As we can see on the XPS graph below, the big peak at 284eV (C-C) and the peak at 286 (C-O-C) are present on the bare gold electrode and can be associated with probable carbon contamination. The post electrodeposition spectrum shows additional peaks around 288eV which is indicative of carboxylic group. We can also observe several eV to higher binding energy of the main peak, a wider peak around 291-292 eV that can be attributed to the aromatic ring in the diazonium structure.

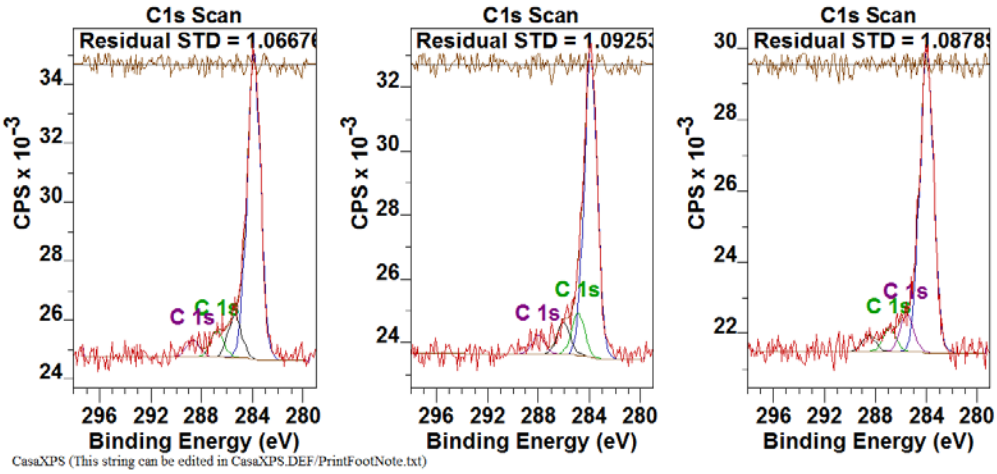

Figure 6.2: Carbon spectra: Au thin film pre-electrografting

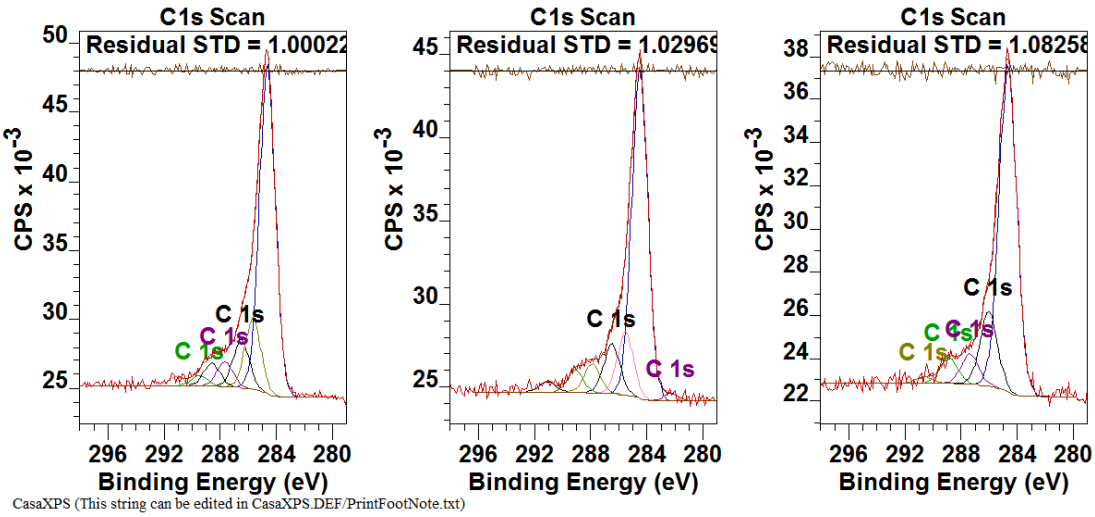

Figure 6.3: Carbon spectra: Au thin film post-electrografting.

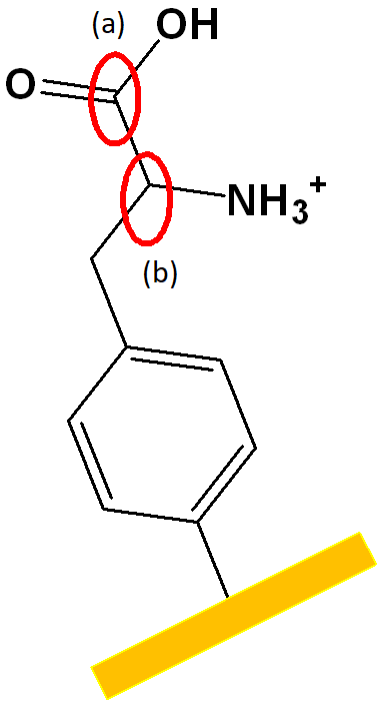

Figure 6.4: Electrografted phenylalanine on gold thin film, (a) carboxylic carbon, (b)amine carbon

As expected, the bare gold sample did not produce a meaningful nitrogen signal (Figure 6.5). The N1s signal is of interest to determine the changes in the gold surface composition post electrografting. The broad peak at 400 eV (Figure 6.6) was decomposed into two peaks that was interpreted as the presence of amine ($-NH_2$) or azo ($-N{=}N-$) groups or both[76–78].

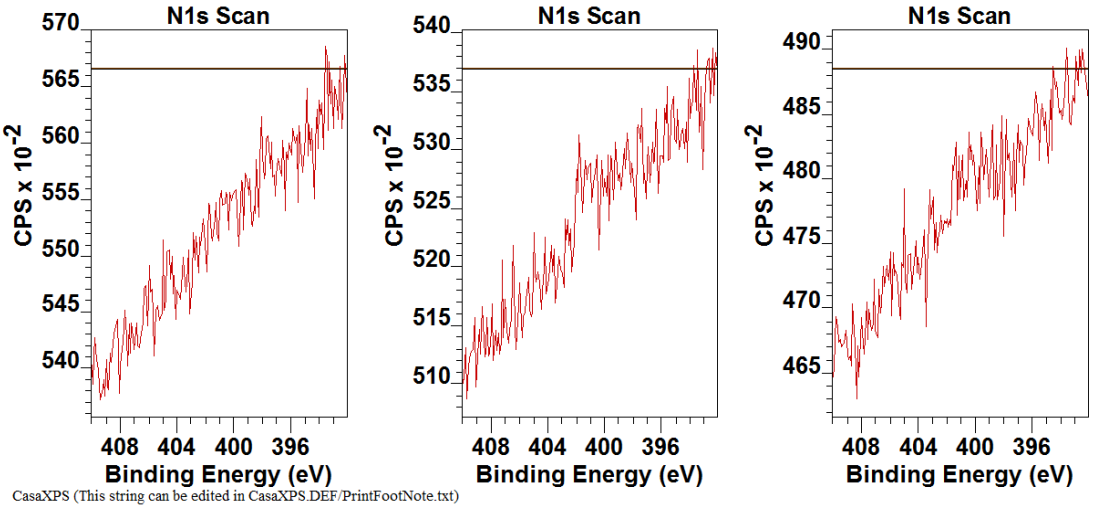

Figure 6.5: Nitrogen spectra: Au thin film pre-electrografting

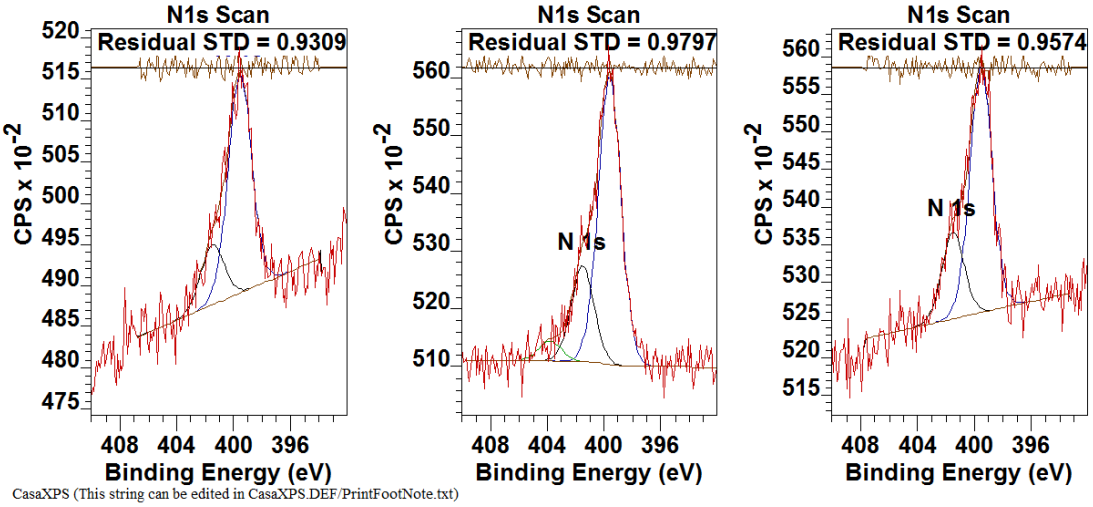

Figure 6.6: Nitrogen spectra: Au thin film post-electrografting

6.3 Contact angle

Contact angle measurements were conducted using KRUSS contact angle instrument to determine whether the hydrophobicity of the gold surface electrode changed upon electrografting modification by 4-aminophenyl alanine. Figure 6.7 and Table 2 summarize the water contact angle measurements on bare gold electrodes surfaces before and after the modification with 4-aminophenylalanne. The water contact angle on a bare gold electrode is about 82° (Figure 6.7 (a)), indicating that the surface is very hydrophobic with poor wetting properties. Once the gold electrode surface is modified with 4-APA, the water contact angle of the coated surface decreases to about 12° (Figure 6.7 (c)). This drop could result from the amphiphilic nature of the peptide molecule imparting hydrophobic moieties to the surface upon the modification. Since the amine group is available for protonation, at physiological pH the electrografted 4-APhe is present in the zwitterionic state. As a consequence, water molecules form a tightly bound hydration layer surrounding the ionic charges in the electrografted 4-APhe, hindering protein adsorption[75].

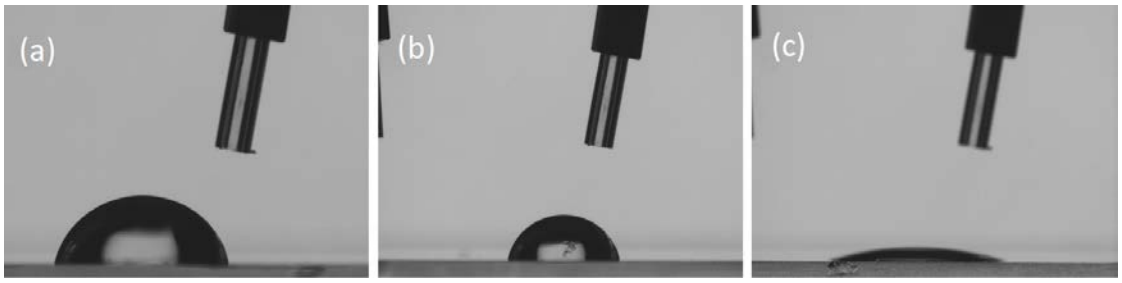

Figure 6.7: Contact angle of different gold thin film: (a)Reference: bare gold film, (b)Immersed: thin film was immersed in 4-amino-L-phenylalanine diazonium, (c)Modified: electrografted thin film with 4-amino-L-phenylalanine diazonium.

Table 6.1: Contact angle summary of Reference, Immersed and Modified gold thin films

Reference				Immersed				Modified			
CA Right	STDV	CA Left	STDV	CA Right	STDV	CA Left	STDV	CA Right	STDV	CA Left	STDV
76.18	2.98	81.56	1.74	77.87	4.42	80.00	1.74	12.30	2.22	11.08	0.88

6.4 Ferri/Ferrocyanide

The density and uniformity of the electrografted layers was evaluated by measuring the peak potential separation (ΔEp) of the ferro/ferricyanide redox couple $Fe(CN)_6^{4-/3-}$ in phosphate buffer solution. Potassium ferricyanide was purchased from EM Science (Gibbstown, NJ), potassium chloride and potassium phosphate monobasic were purchased from Fisher Scientific (Pittsburgh, PA), and sodium chloride and sodium phosphate dibasic heptahydrate were purchased from Mallinckrodt Baker (Paris, KY). The pH of the $Fe(CN)_6^{4-/3-}$ solution was adjusted using sodium hydroxide or hydrochloric acid (both from Fisher Scientific, Pittsburgh, PA) and measured with Mettler Toledo SevenMulti pH meter (Columbus, OH). Cyclic voltammograms of 1.0 mM ferricyanide reagent in 50 mM KCl / 50mM phosphate buffer solution (pH 7) solutions were acquired with the diazonium salt-modified electrodes between -300 mV and +600 mV (vs. Ag/AgCl) at ν = 20mV/s. The peak potential difference increased by 4. 5mV ± 1.82mV. The current difference before electrodeposition was determined to be -0.4083uA and after electrografting was calculated to be 2.3291uA. The increase of the peak currents with successive potential scans indicates that the deposition $4Phe^+$ been achieved[75].

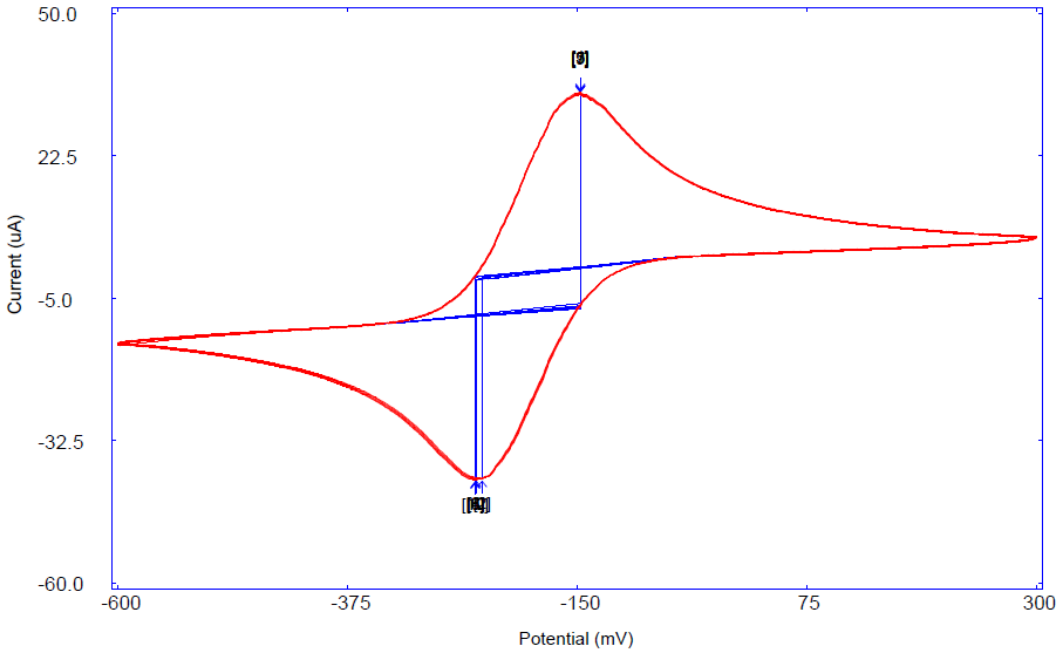

Figure 6.8: Ferri/Ferrocianide pre electrografting cyclic voltammogram; Initial Potential: -600 (mV), Switching Potential 1: 300 (mV), Switching Potential 2: -600 (mV), Final Potential: -600 (mV), Number of segments: 10, Scan rate: 100 (mV/s), Current Full Scale: 100 uA, Filter: 10 Hz, Sample Interval: 1 mV.

Table 6.2: Peak current and potential for bare gold electrode

	Potential (mV)	Current (uA)	Charge (uC)
Peak 1	-147	41.2268	28.6432
Peak 2	-243	38.6389	26.6932
Peak 3	-147	41.6266	29.5070
Peak 4	-249	38.3276	26.5095
Peak 5	-147	41.2787	29.3373
Peak 6	-250	38.3917	26.6791
Peak 7	-147	41.1109	28.9673

Peak 8	-250	39.2096	28.9673
Peak 9	-147	40.3449	28.4033
Peak 10	-250	39.3744	27.8893

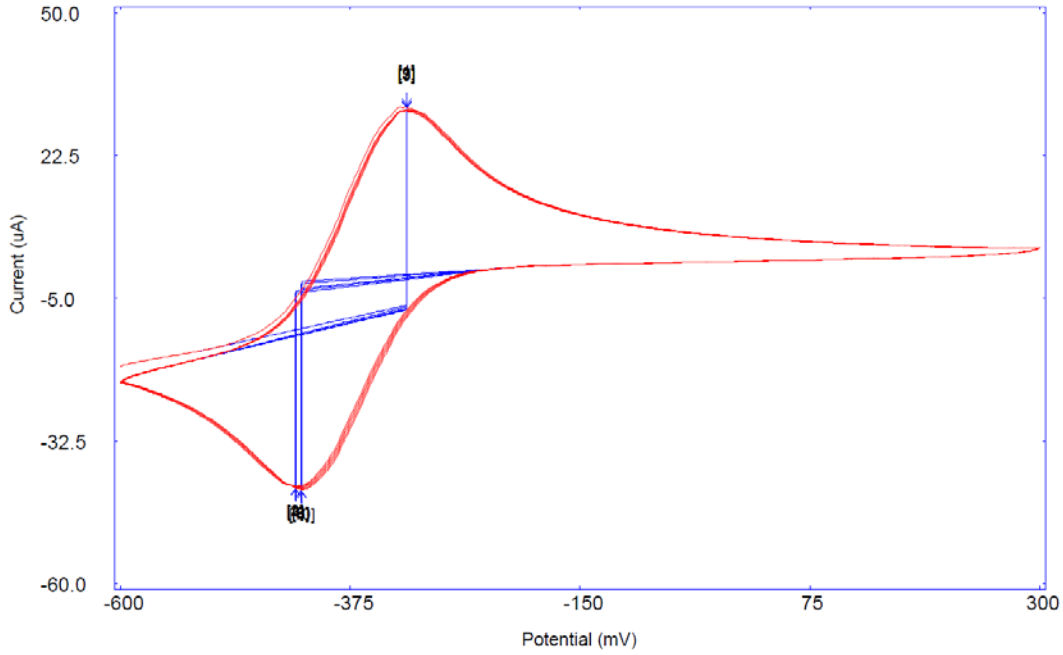

Figure 6.9: Ferri/Ferrocianide post electrografting cyclic voltammogram; Initial Potential: -600 (mV), Switching Potential 1: 300 (mV), Switching Potential 2: -600 (mV), Final Potential: -600 (mV), Number of segments: 10, Scan rate: 100 (mV/s), Current Full Scale: 100 uA, Filter: 10 Hz, Sample Interval: 1 mV.

Table 6.3: Peak current and potential for modified gold electrode

	Potential (mV)	Current (uA)	Charge (uC)
Peak 1	-320	38.2361	26.8853
Peak 2	-429	37.1984	26.8545

Peak 3	-320	38.1476	27.3717
Peak 4	-428	37.7356	27.1323
Peak 5	-320	38.4039	27.5798
Peak 6	-423	38.1933	27.6249
Peak 7	-320	38.1842	27.3571
Peak 8	-423	39.4507	28.8489
Peak 9	-320	37.7234	26.8475
Peak 10	-422	40.1587	29.4786

6.5 Grazing Angle FTIR

The detection and identification of organic layers on reflective surfaces is commonly and rapidly done by FTIR reflective methods. Common FTIR analytical technique instrument configurations are not well suited for analysis of layers on the nanoscale. The HYPERION microscope coupled with Bruker fixed grazing angle objective was used to assess the surface modification from the diazonium electrografting. It is believed that Bruker grazing objectives might be working at its detection limit due to its fixed angle and the low thickness (less than 20nm) of the diazonium film. Spectra collected below showed no successful surface modification, thus not supporting TOF SIMS, XPS, contact angle and SPR data. Menegazzo et al. samples were analyzed in grazing angle specular reflectance mode with an Auto Seagull accessory (Harrick Scientific, Pleasantville, NY) adjusted to a beam incidence of 87° which is higher than the Bruker objective which is believed to be 82.

From the work of Menegazzo et al. Figure 6.4 below shows which bands were expected to be present; they reported that the bands at 1612 cm^{-1} and ~1504cm^{-1} were present on the FTIR spectra and identified as the asymmetric and symmetric δNH_3^+ respectively. The also reported that the bands at 1579 cm^{-1} (CCring), 1117 cm^{-1} (rNH_3^+), and the sequence of peaks between 824 cm^{-1} and 870 cm^{-1}, associated with γCH vibrations of the aromatic ring, all indicated that the overall structure of the precursor was maintained during diazotation and subsequent electrografting. The band centered at 1724 cm^{-1} indicated that νCO bonds were present which translated into the electrografted layers being able to undergo functionalization with bioreceptors using conventional bioconjugation techniques such as EDC/NHS coupling. The band present at ~1440 cm^{-1} was associated to the diazo group (–N=N–) which would be indicative of a multilayered structure[75].

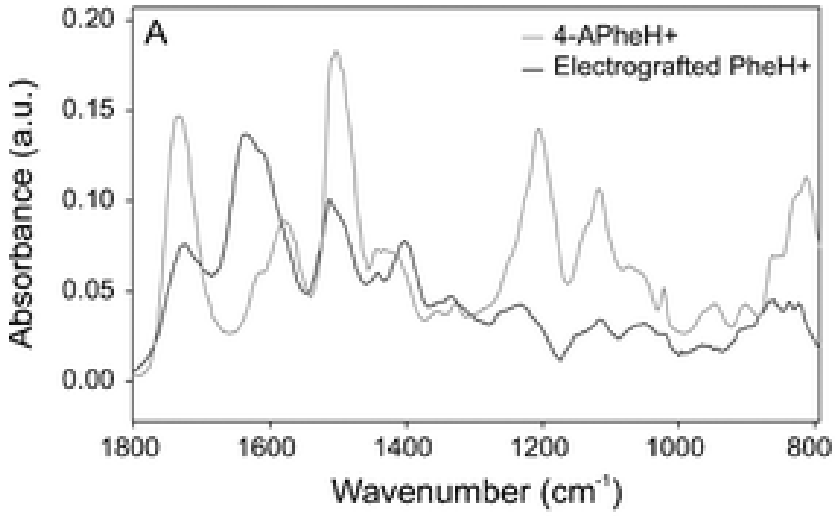

Figure 6.10: Menegazzo et al. (A) Mid-infrared spectrum of 4-$APheH^+$ drop-casted and subsequently allowed to air dry, compared to the spectrum acquired of the electrografted layer[75].

The spectrum collected showed with Bruker objectives showed heavy water pollution. The angle of incidence was concluded to not be suitable for this analysis. The diazonium film thickness was believed to be too low as well due to the difficulties encountered while attempting to measure its thickness using Anasys NanoIR2 which advertised a resonance enhanced mode allowing nanoscale IR on <20nm films.

Chapter 7

PLATFORM PERFORMANCE

Non-specific binding (NSB) refers to the binding of a ligand to something other than its designated receptor. In the case there's no designated receptor no binding should be occurring. Non-specific binding behavior is an important information to acquire in this study and can be used as a measure of the platform performance. In order to assess the successful electrografting of the diazonium salt onto the gold, its antifouling ability was tested using bovine serum albumin

7.1 Bulk Sensitivity

The bulk sensitivity of the homemade SPR instrument was tested using glucose solution of different concentration thus refractive index. 8 solutions were made and their refractive index was recorded using Abbe refractometer. The bulk sensitivity was estimated to be 2047.7.

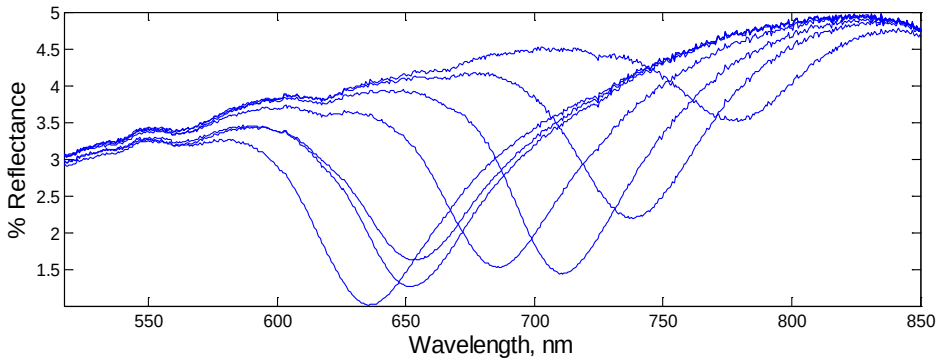

Figure 7.1SPR dip progression resulting from varying concentration of standard sucrose solution

Table 7.1: Sucrose solutions concentration and respective RI

Sucrose solution	Sucrose weight (g)	Final weight (g)	Sucrose solution w%	Sucrose solution RI
1	0.0000	20.000	0.000	1.3315
2	1.0176	20.3502	5.000	1.3390
3	2.0061	20.0338	10.02	1.3460
4	3.005	20.1651	14.90	1.3540
5	4.0159	20.2318	19.85	1.3625
6	5.0006	20.1223	24.85	1.3705
7	6.0041	20.1994	29.72	1.3790
8	7.0043	20.1683	34.73	1.3885

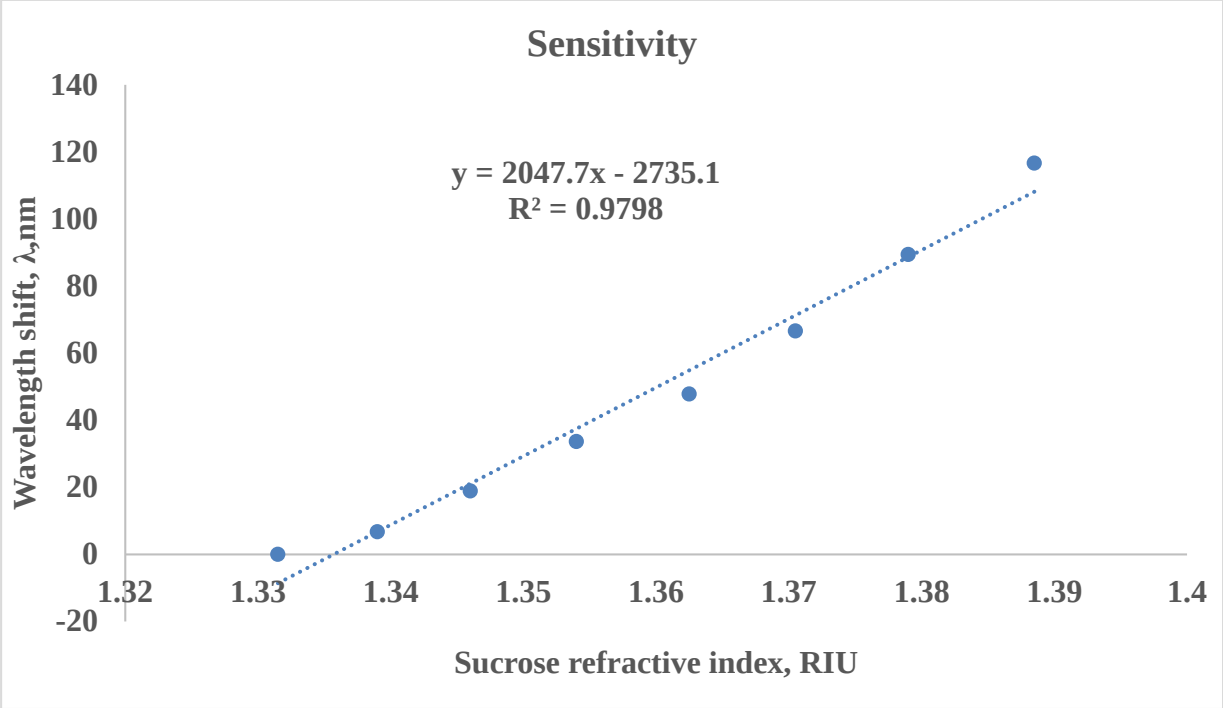

Figure 7.2: Gold bulk sensitivity using varying sucrose concentration/refractive index of sucrose solutions from Table 5.

7.2 EDC/NHS Coupling

The standard amine coupling includes a three-step reaction with EDC/NHS . The reaction step below describes protein immobilization via carboxyl group activation. One very important factor to consider throughout this procedure are the pHs at each step of the reaction chain. The carbonyl activation is favorable at low pHs, preferably between 4-6. At this pH value, the entire residue is protonated. NHS are sufficiently stable to process in a two-step reaction scheme, both groups will hydrolyze within hours or minutes, depending on water-content and pH of the reaction solution. (NHS esters have a half-life of 4-5 hours at pH 7, 1 hour at pH 8 and only 10 minutes at pH 8.6.). The activation reaction with EDC and Sulfo-NHS is most efficient at pH 4.5-7.2, and EDC

reactions are often performed in MES buffer (Product No. 28390) at pH 4.7-6.0. Reaction of Sulfo-NHS-activated molecules with primary amines is most efficient at pH 7-8, and Sulfo-NHS-ester reactions are usually performed in phosphate-buffered saline (PBS) at pH 7.2-7.5. For best results in two-step reactions, perform the first reaction in MES buffer (or other non-amine, non-carboxylate buffer) at pH 5-6, then raise the pH to 7.2-7.5 with phosphate buffer (or other non-amine buffer) immediately before reaction to the amine-containing molecule.

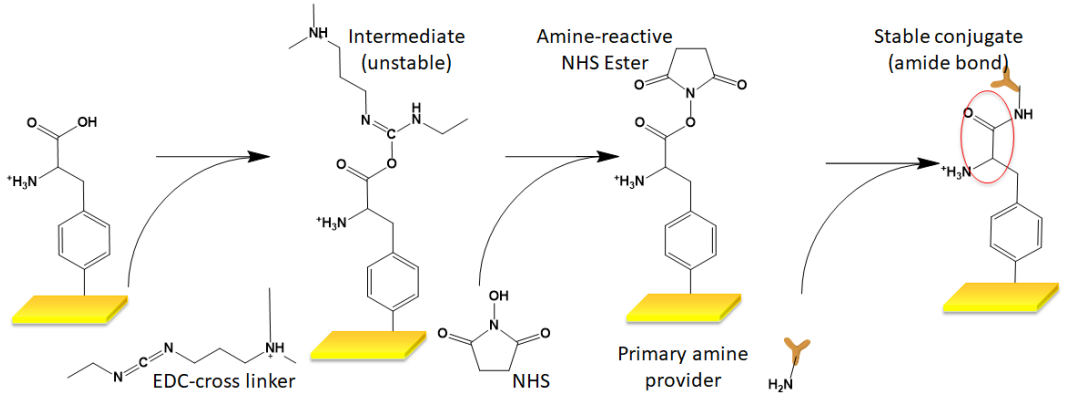

Figure 7.3: EDC/NHS coupling mechanism of 4-amino phenyl alanine and antibody.

7.3 Non-specific binding studies

After the flow cells were made the experiment, two set of experiments were planned. The first part was to assess the NSB layer of the BSA without the antifouling layer and the second with the antifouling layer. On both experiments, water was passed

onto the gold surface followed by PBS then BSA. Later, the gold surface was washed with PBS followed by water. The SPR shift difference determined using MATLAB.

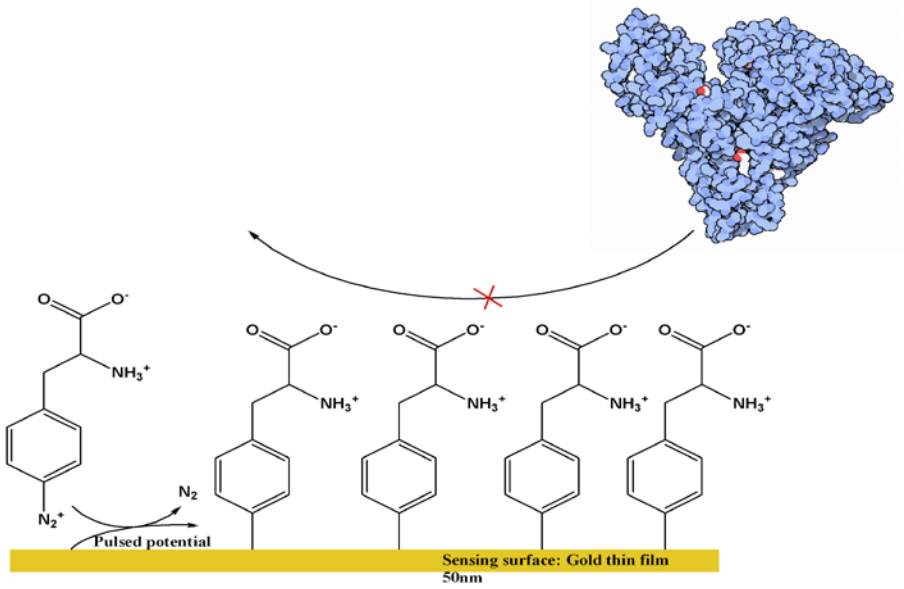

Figure 7.4: Illustration of the diazonium antifouling properties

Table 7.2 SPR dip location and shift of bare gold film

	Initial(nm)	Final(nm)	Difference (nm)
Cell 1	623.10	626.56	3.47
Cell 2	619.20	622.01	2.82
Cell 3	618.18	620.69	2.51
Cell 4	627.08	629.86	2.790

Table 7.3: SPR dip location and shift of modified gold film

	Initial (nm)	Final (nm)	Difference (nm)
Cell 1	629.307	628.66	0.65
Cell 2	627.45	627.91	0.47
Cell 3	612.13	613.88	1.75
Cell 4	631.28	630.91	0.37

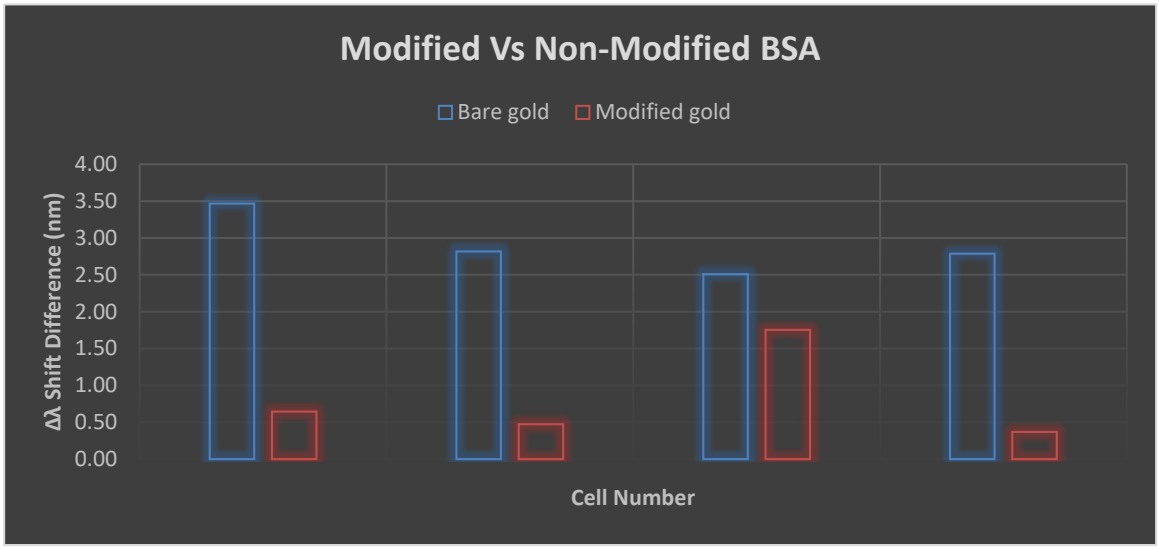

Figure 7.5: SPR red shift difference post exposure of bare and modified gold surface to bovine serum albumin.

On cell 3 we can observe a much higher shift compared to cells 1, 2, and 4. This can be explained by the poor electrografting due to a corrupted reference electrode. The

reference electrode of this cell appeared to be deeply oxidized prior to the chloronizing step compared to the reference electrode on the other platforms.

7.4 Bovine Serum Albumin Immobilization

After the electrografting procedure, a diazonium salt layer with exposed reactive carboxyl groups was obtained. The sensor was equilibrated first in deionized water for 15min, then in MES buffer, pH 5.5 for an additional 15min. A 1:1 solution of 0.4M N-(3-dimethylaminopropyl)-N′-ethylcarbodiimide (EDC, 99%, Sigma-Aldrich) and 0.01M N-hydroxysuccinimide (NHS, 98%, Fisher Scientific) was reacted for 5min. The EDC/NHS mixture was injected into the flowcell for 1min before being stopped and left to react with the diazonium exposed carboxyl for 15min at room temperature. The pH chosen for the immobilization procedure plays a critical role in its success. For the reaction with the activated ester to occur, Figure 7.3, the ligand has to be uncharged and brought in close proximity of the surface by a process called preconcentration. BSA pI (isoelectric point) is around 4.7, thus the activated surface was then allowed to react with 1mg/mL concentrated BSA solution, mixed in acetate buffer pH 4.7, that was injected into the cell for 1min before the pump was stopped. BSA was allowed to interact with the activated surface for 1h at room temperature[79]. The sensor was then flushed with PBS pH 7.4 for 1min to remove non-specifically bound proteins. The non-reacted sites (carboxyl groups) of the gold surface were deactivated by using a 1.0M solution of ethanolamine at pH 8.5 for 15min. The sensor was then flush with PBS buffer, pH 7.4, 3 times in 5min intervals for a period of 3min before being allowed to equilibrate for 15min. A calculated red shift of a 2.33 nm was observed after immobilization of BSA.

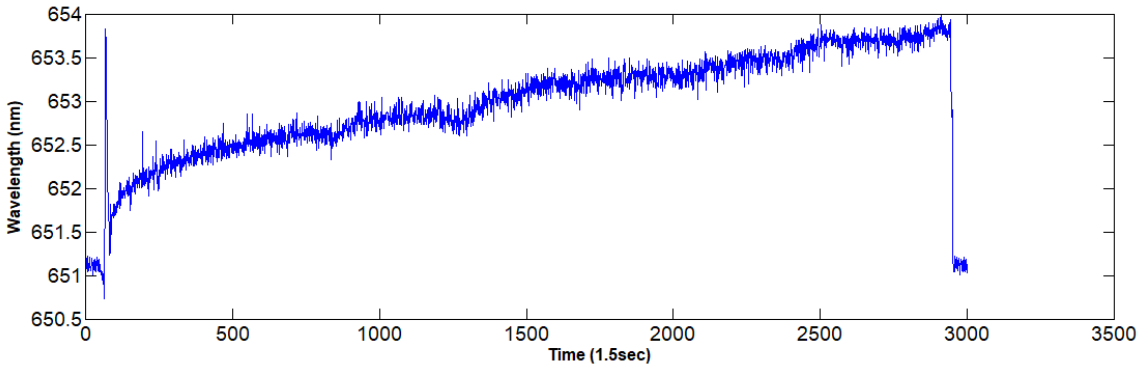

Figure 7.6: SPR preliminary sensorgram of bovine serum albumin immobilization post electrografting and surface exposure to EDC/NHS

7.5 Bovine serum albumin antibody (ABSA) immobilization

As mentioned in the previous section, a diazonium salt layer with exposed reactive carboxyl groups was obtained after electrografting procedure. The same immobilization procedure was followed but different a buffer pH was used. The sensor was equilibrated first in deionized water for 15min, then in PBS, pH 7.4 for an additional 15min. A 1:1 solution of 0.4M N-(3-dimethylaminopropyl)-N′-ethylcarbodiimide (EDC, 99%, Sigma-Aldrich) and 0.1M N-hydroxysuccinimide (NHS, 98%, Fisher Scientific) was reacted for 5min. The EDC/NHS mixture was injected into the flowcell for 3min before being stopped and left to react with the diazonium exposed carboxyl for 20min at room temperature. The activated surface was then allowed to react with 100µg/mL ABSA solution, mixed in PBS buffer pH 7.4, that was injected into the cell for 3min before the pump was stopped. ABSA was allowed to interact with the activated surface for 1h at room temperature. The sensor was then flushed with PBS pH 7.4 for

3min to remove non-specifically bound proteins. The non-reacted sites (carboxyl groups) of the gold surface were then deactivated by using a 1.0 M solution of ethanolamine at pH 8.5 for 15min. The sensor was then flush with PBS buffer, pH 7.4, 3 times in 5min intervals for a period of 3min before being allowed to equilibrate for 15min.

7.6 Selective electrodeposition

The selective electrografting of diazonium salt layers onto the gold surface permits the individual modification of the reference and analytical SPR sensors within a single channel. Established instrumentation like BIACore, make use of a separate reference channel to compensate for background effects as nonspecific binding and temperature fluctuations. Zou et al. work was adapted to the platform to help the integration of an in-channel referencing pad[80]. The sensorgram presented below depicts the electrografting progression of 4Phe on a single pad within the same analysis channel. The blue line represents the referencing pad and the red line the sensing pad. This experiment was conducted at room temperature of 19C. From the electrografted pad we observed a red shift of 10nm while the referenced pad that was just immersed in the solution shows a slight red shift of less than 2nm, which can be associated with non-specific binding. The sensorgram below agrees with the contact angle and XPS data presented prior.

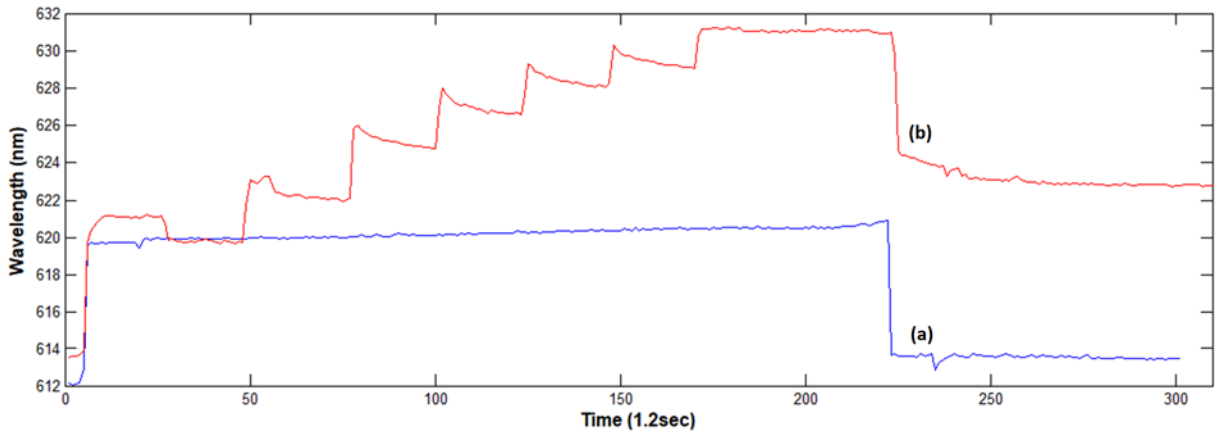

Figure 7.7: Selective electrografting sensorgram of 4-amino phenyl alanine diazonium: (a) bare gold electrode, (b) modified gold electrode

Chapter 8

CONCLUDING REMARKS

This project mainly focused on the fabrication of a platform that would be suitable for the development of an EK-SPR biosensor. The proper conditions for the thin film deposition were investigated after encountering difficulties with the in-house deposition instrument: Cressington 328. The University of Delaware Nanofabrication facility was used for the metal deposition. The diazonium salt of 4-aminophenylalanaine which is a derivative of the amino acid phenyl alanine was grafted onto the gold electrode of interest with chrono-amperometry or cyclic voltammetry. The platform showed some potential but more investigational and optimization work needs to be done towards surface characterization and the fluidics in order to eliminate air bubbles and delaminating PDMS during the analysis. One of the mile stone accomplished during this investigation was the fabrication of a 3 - electrodes thin film system that integrate an in-channel referencing pad. The current design allowed the real time monitoring of the electrografting progression. Menegazzo et al. framework was followed during this project. The antifouling properties of the diazonium layer was verified by doing an antifouling study. Bovine serum albumin was the protein used during this investigational work to test the platform potential. Preliminary preconcentration data using the developed platform and Bovine Serum Albumin (BSA) Alexa Fluor 488 conjugate were obtain by William Gilbraith of the Booksh group. The collected data contributed to support the potential of this platform to be optimized for EK-SPR. The analytical figures if merit for the platform still need to be established after the fluidics of the platform has been updated. A possible remedy to the delamination of the PDMS,

which causes the cell prototype to leak during the analysis, is to investigate the use a different flowcell material such as poly(methyl methacrylate) (PMMA).

REFERENCES

1. Benjamin, E. J. *et al.* Heart disease and stroke statistics - 2018 update: A report from the American Heart Association. *Circulation* **137**, E67–E492 (2018).

2. Overbaugh, B. K. J. ACUTE ORONARY Syndrome. *Ajnr* **109**, 42–52 (2009).

3. Smith, J. N., Negrelli, J. M., Manek, M. B., Hawes, E. M. & Viera, A. J. Diagnosis and Management of Acute Coronary Syndrome: An Evidence-Based Update. *The Journal of the American Board of Family Medicine* **28**, 283–293 (2015).

4. Yang, Z. & Min Zhou, D. Cardiac markers and their point-of-care testing for diagnosis of acute myocardial infarction. *Clinical Biochemistry* **39**, 771–780 (2006).

5. Pope, H. J. *et al.* Missed Diagnoses of Acute Cardiac Ischemia in the Emergency Department. *The New England Journal of Medicine* **342**, 1163–1170 (2000).

6. WHO | Top 10 causes of death. *WHO* (2018).

7. Mythili, S. & Malathi, N. Diagnostic markers of acute myocardial infarction (Review). *Biomedical Reports* **3**, 743–748 (2015).

8. Eisenman, A. Troponin assays for the diagnosis of myocardial infarction and acute coronary syndrome: where do we stand? *Expert Review of Cardiovascular Therapy* **4**, 509–514 (2006).

9. Newby, L. K. *et al.* Comparison of cardiac troponin T versus creatine kinase-MB for risk stratification in a chest pain evaluation unit. *The American Journal of Cardiology* **85**, 801–5 (2000).

10. Apple, F. S. & Murakami, M. M. Cardiac Troponin and Creatine Kinase MB Monitoring during In-Hospital Myocardial Reinfarction. *Clinical Chemistry* **51**, 460–463 (2005).

11. Bonham, M. & Miller, S. Clinical Comparison of 99th Percentile and 10% Coefficient of Variation Cutoff Values for Four Commercially Available

Troponin I Assays. *Laboratory Medicine* **40**, 470–473 (2009).

12. Amundson, B. E. & Apple, F. S. Cardiac troponin assays: A review of quantitative point-of-care devices and their efficacy in the diagnosis of myocardial infarction. *Clinical Chemistry and Laboratory Medicine* **53**, 665–676 (2015).

13. Melanson, S. E. F., Tanasijevic, M. J. & Jarolim, P. Cardiac troponin assays: A view from the clinical chemistry laboratory. *Circulation* **116**, 501–504 (2007).

14. Garg, P. *et al.* Cardiac biomarkers of acute coronary syndrome: from history to high-sensitivity cardiac troponin. *Internal and Emergency Medicine* **12**, 147–155 (2017).

15. Health, C. for D. and R. In Vitro Diagnostics. Available at: https://www.fda.gov/medicaldevices/productsandmedicalprocedures/invitrodiagnostics/default.htm. (Accessed: 22nd November 2018)

16. *Point-of-Care/Rapid Diagnostics Market by Testing (Glucose, Lipids, HbA1c, HCV, HIV, Influenza, Urinalysis, Hematology, Cancer, Pregnancy, PT/INR), Platform (Lateral Flow, Immunoassay), Mode (Prescription, OTC), End-User - Global Forecast to 2022*. (2018).

17. Unold, D. & Nichols, J. H. Point-of-Care Testing: Needs, Opportunity, and Innovation, 3rd Edition, by Christopher P. Price, Andrew St John, and Larry J. Kricka, eds. *Clinical Chemistry* **56**, 1893–1894 (2010).

18. Peeling, R. W., Holmes, K. K., Mabey, D. & Ronald, A. Rapid tests for sexually transmitted infections (STIs): the way forward. *Sexually Transmitted Infections* **82 Suppl 5**, v1-6 (2006).

19. Hsieh, Y.-H. *et al.* What Qualities Are Most Important to Making a Point of Care Test Desirable for Clinicians and Others Offering Sexually Transmitted Infection Testing? *PLoS ONE* **6**, 1–5 (2011).

20. St John, A. & Price, C. P. Point-of-Care Testing Technologies Clin Biochem Rev 35 (3) 2014 155 Existing and Emerging Technologies for Point-of-Care Testing. *Clinical Biochemistry Review* **35**, 155–167 (2014).

21. Wang, L., Yin, H. & Cheng, J. From biochips to laboratory-on-a-chip system. *Genomic signal processing and statistics* 449 (2005).

22. Johnson, A. S., Mehl, B. T. & Scott Martin, R. Integrated hybrid polystyrene-polydimethylsiloxane device for monitoring cellular release with microchip

electrophoresis and electrochemical detection. *Analytical Methods* **7**, 884–893 (2015).

23. Choi, J. R. *et al.* Paper-based sample-to-answer molecular diagnostic platform for point-of-care diagnostics. *Biosensors and Bioelectronics* **74**, 427–439 (2015).

24. Hu, J. *et al.* Advances in paper-based point-of-care diagnostics. *Biosensors and Bioelectronics* **54**, 585–597 (2014).

25. You, M. *et al.* Household Fluorescent Lateral Flow Strip Platform for Sensitive and Quantitative Prognosis of Heart Failure Using Dual-Color Upconversion Nanoparticles. *ACS Nano* **11**, 6261–6270 (2017).

26. Koczula, K. M. & A., G. Lateral flow assays. *Essays in Biochemistry* **60**, 111–120 (2016).

27. García-Basteiro, A. L. *et al.* Point of care diagnostics for tuberculosis. *Revista Portuguesa de Pneumologia (English Edition)* **24**, 73–85 (2018).

28. Xu, X. *et al.* Advances in Smartphone-Based Point-of-Care Diagnostics. *Proceedings of the IEEE* **103**, 236–247 (2015).

29. Antman, E. *et al.* Myocardial infarction redefined—a consensus document of The Joint European Society of Cardiology/American College of Cardiology committee for the redefinition of myocardial infarction: The Joint European Society of Cardiology/ American College of Cardiology Committee. *Journal of the American College of Cardiology* **36**, 959–969 (2000).

30. GENWAY BIOTECH INC. Sandwich ELISA. Available at: https://www.genwaybio.com/services/sandwich-elisa. (Accessed: 22nd November 2018)

31. Aydin, S. A short history, principles, and types of ELISA, and our laboratory experience with peptide/protein analyses using ELISA. *Peptides* **72**, 4–15 (2015).

32. Eteshola, E. & Leckband, D. Development and characterization of an ELISA assay in PDMS microfluidic channels. *Sensors and Actuators, B: Chemical* **72**, 129–133 (2001).

33. Cho, I. H., Paek, E. H., Kim, Y. K., Kim, J. H. & Paek, S. H. Chemiluminometric enzyme-linked immunosorbent assays (ELISA)-on-a-chip biosensor based on cross-flow chromatography. *Analytica Chimica Acta* **632**,

247–255 (2009).

34. Wu, W. Y., Bian, Z. P., Wang, W., Wang, W. & Zhu, J. J. PDMS gold nanoparticle composite film-based silver enhanced colorimetric detection of cardiac troponin I. *Sensors and Actuators, B: Chemical* **147**, 298–303 (2010).

35. Coons, A. H., Creech, H. J. & Jones, R. N. Immunological Properties of an Antibody Containing a Fluorescent Group. *Experimental Biology and Medicine* **47**, 200–202 (1941).

36. Wu, A. H. B., Fukushima, N., Puskas, R., Todd, J. & Goix, P. Development and preliminary clinical validation of a high sensitivity assay for cardiac troponin using a capillary flow (single molecule) fluorescence detector. *Clinical chemistry* **52**, 2157–9 (2006).

37. Tate, J., Barth, J. & Bunk, D. *Table. Analytical characteristics of commercial and research cardiac troponin I and T assays declared by the manufacturer*. (2012).

38. Luxton, R., Badesha, J., Kiely, J. & Hawkins, P. Use of External Magnetic Fields to Reduce Reaction Times in an Immunoassay Using Micrometer-Sized Paramagnetic Particles as Labels (Magnetoimmunoassay). *Analytical Chemistry* **76**, 1715–1719 (2004).

39. Eveness, J., Kiely, J., Hawkins, P., Wraith, P. & Luxton, R. Evaluation of paramagnetic particles for use in a resonant coil magnetometer based magneto-immunoassay. *Sensors and Actuators, B: Chemical* **139**, 538–542 (2009).

40. Pankhurst, Q. A., Connolly, J., Jones, S. K. & Dobson, J. Applications of magnetic nanoparticles in biomedicine. *Journal of Physics D: Applied Physics* **36**, 167–181 (2003).

41. Senyei, A., Widder, K. & Czerlinski, G. Magnetic guidance of drug-carrying microspheres. *Journal of Applied Physics* **49**, 3578–3583 (1978).

42. Bruls, D. M. *et al.* Rapid integrated biosensor for multiplexed immunoassays based on actuated magnetic nanoparticles. *Lab on a Chip* **9**, 3504–3510 (2009).

43. Kiely, J., Hawkins, P. & Luxton, R. Paramagnetic particle detection for use with an immunoassay based biosensor. *IET Science, Measurement & Technology* **1**, 270–275 (2007).

44. Todd, J. *et al.* Ultrasensitive flow-based immunoassays using single-molecule counting. *Clinical Chemistry* **53**, 1990–1995 (2007).

45. Sauerbrey, G. The use of quartz oscillators for weighing thin layers and for microweighing. *Zeitschrift Für Physik* 206–222 (1959).

46. Wong-ek, K., Chailapakul, O., Nuntawong, N., Jaruwongrungsee, K. & Tuantranont, A. Cardiac troponin T detection using polymers coated quartz crystal microbalance as a cost-effective immunosensor. *Biomedizinische Technik. Biomedical engineering* **55**, 279–84 (2010).

47. Lee, J. *et al.* Sensitive and Simultaneous Detection of Cardiac Markers in Human Serum Using Surface Acoustic Wave Immunosensor. *Analytical Chemistry* **83**, 8629–8635 (2011).

48. Chekin, F. *et al.* Sensitive electrochemical detection of cardiac troponin I in serum and saliva by nitrogen-doped porous reduced graphene oxide electrode. *Sensors and Actuators, B: Chemical* **262**, 180–187 (2018).

49. Ahammad, A. J. S. *et al.* Electrochemical detection of cardiac biomarker troponin I at gold nanoparticle-modified ITO electrode by using open circuit potential. *International Journal of Electrochemical Science* **6**, 1906–1916 (2011).

50. Shan, M. *et al.* Sensitive electrogenerated chemiluminescence peptide-based biosensor for the determination of troponin i with gold nanoparticles amplification. *Gold Bulletin* **47**, 57–64 (2014).

51. Mohammed, M. I. & Desmulliez, M. P. Y. Lab-on-a-chip based immunosensor principles and technologies for the detection of cardiac biomarkers: A review. *Lab on a Chip* **11**, 569–595 (2011).

52. Masson, J. F., Obando, L., Beaudoin, S. & Booksh, K. Sensitive and real-time fiber-optic-based surface plasmon resonance sensors for myoglobin and cardiac troponin I. *Talanta* **62**, 865–870 (2004).

53. Kwon, Y. C. *et al.* Development of a surface plasmon resonance-based immunosensor for the rapid detection of cardiac troponin I. *Biotechnology Letters* **33**, 921–927 (2011).

54. Pawula, M., Altintas, Z. & Tothill, I. E. SPR detection of cardiac troponin T for acute myocardial infarction. *Talanta* **146**, 823–830 (2016).

55. Wood, R. On a Remarkable Case of Uneven Distribution of Light in a Diffraction Grating Spectrum. *Philosophical Magazine* **18**, 396–402 (1902).

56. Wood, R. W. XXVII. Diffraction gratings with controlled groove form and

abnormal distribution of intensity. *The London, Edinburgh, and Dublin Philosophical Magazine and Journal of Science* **23**, 310–317 (1912).

57. Otto, A. Excitation of nonradiative surface plasma waves in silver by the method of frustrated total reflection. *Zeitschrift für Physik A Hadrons and nuclei* **216**, 398–410 (1968).

58. Kretschmann, E. & Raether, H. Notizen: Radiative Decay of Non Radiative Surface Plasmons Excited by Light. *Zeitschrift für Naturforschung A* **23**, 2135–2136 (1968).

59. Rayleigh, L. On the Dynamical Theory of Gratings. *Proceedings of the Royal Society A: Mathematical, Physical and Engineering Sciences* **79**, 399–416 (1907).

60. Anal, A. K. Types of Antibody -Based Biosensors. in *Bionanotechnology: Principles and Applications* (CRC Press, Taylor & Francis Group, 2018).

61. Barnes, W. L., Dereux, A. & Ebbesen, T. W. Surface plasmon subwavelength optics. *Nature* **424**, 824–830 (2003).

62. Abdulhalim, I., Zourob, M. & Lakhtakia, A. Surface Plasmon Resonance for Biosensing: A Mini-Review. *Electromagnetics* **28**, 214–242 (2008).

63. Schasfoort, R. B. M. History and Physics of Surface Plasmon Resonance. in *Handbook of Surface Plasmon Resonance* 27–59 (Royal Society of Chemistry, 2017).

64. Couture, M., Zhao, S. S. & Masson, J. F. Modern surface plasmon resonance for bioanalytics and biophysics. *Physical Chemistry Chemical Physics* **15**, 11190–11216 (2013).

65. Luka, G. *et al.* Microfluidics integrated biosensors: A leading technology towards lab-on-A-chip and sensing applications. *Sensors (Switzerland)* **15**, 30011–30031 (2015).

66. Thévenot, D. R., Toth, K., Durst, R. A. & Wilson, G. S. Electrochemical biosensors: recommended definitions and classification. *Analytical Letters* **34**, 635–659 (2001).

67. Dutta, G. & Lillehoj, P. B. An ultrasensitive enzyme-free electrochemical immunosensor based on redox cycling amplification using methylene blue †. *Analyst* **142**, 3492 (2017).

68. National Research Council (U.S.). Committee on New Sensor Technologies: Materials and Applications. *Expanding the vision of sensor materials*. (National Academy Press, 1995).

69. Wang, D. S. & Fan, S. K. Microfluidic surface plasmon resonance sensors: From principles to point-of-care applications. *Sensors (Switzerland)* **16**, 1–18 (2016).

70. Becker, H. & Locascio, L. E. Polymer microfluidic devices. *Talanta* **56**, 267–287 (2002).

71. Meighan, M. M., Keebaugh, M. W., Quihuis, A. M., Kenyon, S. M. & Hayes, M. A. Electrophoretic exclusion for the selective transport of small molecules. *Electrophoresis* **30**, 3786–3792 (2009).

72. Kenyon, S. M., Weiss, N. G. & Hayes, M. A. Using electrophoretic exclusion to manipulate small molecules and particles on a microdevice. *Electrophoresis* **33**, 1227–1235 (2012).

73. Meighan, M. M., Vasquez, J., Dziubcynski, L., Hews, S. & Hayes, M. A. Investigation of Electrophoretic Exclusion Method for the Concentration and Differentiation of Proteins. *Analytical Chemistry* **83**, 368–373 (2011).

74. Gibson, I., Rosen, D. W. & Stucker, B. Generalized Additive Manufacturing Process Chain. in *Additive Manufacturing Technologies* 59–77 (Springer US, 2010). doi:10.1007/978-1-4419-1120-9_3

75. Menegazzo, N., Zou, Q. & Booksh, K. S. Characterization of electrografted 4-aminophenylalanine layers for low non-specific binding of proteins. *New Journal of Chemistry* **36**, 963 (2012).

76. Stéphanie Betelu, S. *et al.* Evidence of the Grafting Mechanisms of Diazonium Salts on Gold Nanostructures. *The Journal of Physical Chemistry C* **120**, 18158–18166 (2016).

77. Mooste, M. *et al.* Electrochemical properties of gold and glassy carbon electrodes electrografted with an anthraquinone diazonium compound using the rotating disc electrode method. *RSC Advances* **6**, 40982–40990 (2016).

78. Ortiz, B., Saby, C., Champagne, G. Y. & Bélanger, D. Electrochemical modification of a carbon electrode using aromatic diazonium salts. 2. Electrochemistry of 4-nitrophenyl modified glassy carbon electrodes in aqueous media. *Journal of Electroanalytical Chemistry* **455**, 75–81 (1998).

79. Ge, W.-H., Lin, Y., Li, S., Zong, X. & Ge, Z.-C. Identification of Biomarkers for Early Diagnosis of Acute Myocardial Infarction. *Journal of Cellular Biochemistry* **119**, 650–658 (2018).

80. Zou, Q., Menegazzo, N. & Booksh, K. S. Development and Investigation of a Dual-Pad In-Channel Referencing Surface Plasmon Resonance Sensor. *Analytical Chemistry* **84**, 7891–7898 (2012).